SYNTHESIS AND CHARACTERIZATION OF METAKAOLIN, FLY ASH AND RED MUD BASED GEOPOLYMERS

by

Işıl Özer

B.S., Chemical Engineering, Istanbul Technical University, 2012

Submitted to the Institute for Graduate Studies in
Science and Engineering in partial fulfillment of
the requirements for the degree of
Master of Science

Graduate Program in Chemical Engineering

Boğaziçi University

2015

to my sister

ACKNOWLEDGEMENTS

Firstly, I would like to voice my gratitude to my supervisor Assist. Prof. Sezen Soyer Uzun for her interest, patience, support and geniality throughout my study.

Furthermore, I am grateful to Assist. Prof. Alper Uzun and Melike Babucci for their help and patience in spectroscopy measurements.

Also, my thanks go to Prof. Turan Özturan and Assoc. Prof. Nilüfer Özyurt Zihnioğlu for their interest, Abdullah Huzeyfe Akça and Onur Pehlivan for their technical assistance and patience during compressive strength measurements.

I would like to thank Bilgi Dedeoğlu, Murat Düzgünoğlu, Yakup Bal and Belgin Balkan and Melike Gürbüz for their technical support, kindness and help.

I also want to thank Kardelen Kaya, Ece Küçük and Tuğçe Aygör for their help and patience during my thesis study.

I express thanks to Caner Dalkıç who gives a novel touch to my life and always stands by me, in good and bad days. I am also thankful to Esra Çoban who is my best friend and listens to me all the time and whom I have a great time with.

I am very grateful to my family for their spiritual and material support throughout my life. They always contributed to all my success and trust me with eveything. I am also very thankful to the Tutucus who have supported me throughout my undergraduate and graduate education. Finally, this thesis is devoted to my sister, Eda Özer who is always with me and strikes a happy note.

The financial support for this thesis was supported by Bogazici University Research Fund through Project BAP13A05P5.

ABSTRACT

SYNTHESIS AND CHARACTERIZATION OF METAKAOLIN, FLY ASH AND RED MUD BASED GEOPOLYMERS

Geopolymers stand as potential future alternatives to ordinary cement offering to reduce global CO_2 emissions with added advantages such as better mechanical strength and increased design lives. In this thesis, metakaolin, fly ash (C type), and fly ash-red mud based geopolymers were synthesized, mechanically tested and characterized in detail by spectroscopy, diffraction and microscopy techniques. In the first part of this thesis, metakaolin-based geopolymers with molar Si/Al ratios of 1.12, 1.77 and 2.20 were investigated. Geopolymer samples with Si/Al ratio of 1.12 contained crystalline components, namely zeolite A and/or sodalite phases, whereas geopolymers with Si/Al ratio of 1.77 and 2.20 were mainly 'x-ray amorphous'. The position and width of the main band in FTIR spectra was found to systematically increase with increasing molar Si/Al ratio. The intensity of this band decreased with increasing Si content in the system indicating increased geopolymerization. Compressive strength of these samples were also found to increase systematically with increasing molar Si/Al ratio. The second part of this thesis focused on fly ash and fly ash-red mud based geopolymers. The FTIR spectra of fly-ash based geopolymers with molar Si/Al ratio of 1.95 exhibited the presence of mainly two bands positioned at 941 cm^{-1} and 1099 cm^{-1}. These bands possibly indicated i) a CASH and/or CSH gel and ii) NASH gel, respectively. These gel phases are also observed in SEM images of these specimens. Increasing Si/Al ratio up until 2.40 results in the merging of these bands together. The corresponding compressive strength values seem to increase with increasing Si/Al ratio. On the other hand, fly ash-red mud based geopolymers with low red mud contents reveal similar phase separated structure as evident from FTIR spectroscopy. However, as red mud content increases in the system, two bands corrresponding to CASH and/or CSH gel and NASH gel merge into a broader single feature. Transition from a two-phase structure into a relatively more uniform one should be responsible in corresponding increases in the measured compressive strength values.

ÖZET

METAKAOLİN, UÇUCU KÜL VE KIRMIZI ÇAMUR BAZLI JEOPOLİMERLERİN SENTEZİ VE KARAKTERİZASYONU

Jeopolimerler daha iyi mekanik dayanıklılık ve artan tasarım ömürleri gibi avantajlarıyla global karbondioksit emisyonunu azaltmak için çimentoya gelecekteki potansiyel alternatif aday olmaktadır. Bu tezde metakaolin, uçucu kül (C sınıfı) ve uçucu kül-kırmızı çamur bazlı jeopolimerler sentezlenmiştir, mekanik olarak test edilmiştir ve spektroskopi, difraksiyon ve mikroskopi teknikleri ile detaylıca karakterize edilmiştir. Tezin ilk bölümünde Si/Al mol oranları 1.12, 1.77 ve 2.20 olan metakaolin bazlı jeopolimerler incelenmiştir. Si/Al molar oranı 1.12 olan metakaolin bazlı jeopolimerler zeolite A ve/ya sodalit gibi kristal fazları içermektedir. Ancak, Si/Al mol oranları 1.77 ve 2.20 olan jeopolimer örnekleri büyük oranda x-ray amorf yapıdadır. Metakaolin bazlı numunelerde örneklere ait FTIR spektroskopisindeki ana bandın pozisyonu ve genişliği Si/Al molar oranı arttıkça sistematik olarak artmaktadır. Bu bandın keskinliğinin sistemdeki Si içeriğinin artışıyla azalması jeopolimerizasyonun artmasını göstermiştir. Bu örneklerin basınç dayanımlarının da Si/Al molar oranı arttıkça sistematik olarak arttığı bulunmuştur. Tezin ikinci bölümünde uçucu kül ve uçucu kül-kırmızı çamur bazlı jeopolimerlere odaklanılmıştır. Si/Al mol oranı 1.95 olan uçucu kül bazlı jeopolimere ait FTIR spektroskopisi 941 cm^{-1} and 1099 cm^{-1}'de konumlanan asıl iki bandın varlığını göstermiştir. Bu bandlar muhtemelen sırasıyla i) CASH ve/ya CSH ve ii) NASH jellerini göstermektedir. Bu jel fazları numunelerin SEM görüntülerinde de gözlenmiştir. Si/Al mol oranının 2.40'a kadar artması bu bandların birleşmesiyle sonuçlanmıştır. Basınç dayanım değerlerinin Si/Al mol oranları arttıkça arttığı görülmüştür. Öte yandan, düşük oranda kırmızı çamur içeren uçucu kül-kırmızı çamur bazlı jeopolimerler FTIR sprektroskopisinde kanıtlanan benzer ayrılmış faz yapılarını ortaya çıkarmıştır. Ancak, sistemdeki kırmızı çamur içeriği arttıkça CASH ve/ya CSH ve NASH jellerine karşılık gelen iki band daha geniş tek bir banda dönüşmüştür. İki fazlı yapıdan daha kararlı bir yapıya dönüşüm, ölçülen basınç dayanım değerlerindeki ilgili artıştan sorumlu olmalıdır.

TABLE OF CONTENTS

LIST OF FIGURES

LIST OF TABLES

LIST OF ACRONYMS/ABBREVIATIONS

Al	Aluminum
Al_2O_3	Aluminum oxide
CASH	Calcium aluminosilicate hydrate
CSH	Calcium silicate hydrate
NASH	Aluminium silicate hydrate
CO_2	Carbondioxide
FTIR	Fourier transform infrared spectroscopy
NaOH	Sodium hydroxide
$Na_2Si_3O_7$	Sodium silicate
SEM	Scanning electron microscopy
Si	Silicon
SiO_2	Silicon dioxide
Wt	Weight
XRD	X-ray diffraction

1. INTRODUCTION

The climate change due to global warming is a vital threat to the whole world. The greenhouse gases such as carbon dioxide emitted through human activities lead to global warming. CO_2 has the greatest impact on global warming among greenhouse gases which is responsible of about 65 % of global warming [1,2]. CO_2 level in air has risen from 315 ppm to 365 ppm between 1960 and 2000 [3]. Two billion tonnes of CO_2 per year are emitted in cement production. It is estimated that 3.5 billion tones of CO_2 will be produced annually by cement industry in ten years [3]. The production of portland cement contributes to 5-7 % of global CO_2 emissions [4-6]. Therefore, it is fair to mention that cement manufacturing process increases environmentally unfriendly green house gas emissions [7,8,2].

Recent academic studies have started to focus on 'geopolymers' that are inorganic polymers that arise as potential future alternatives to cement-based materials. Geopolymer was first contrived by Prof. Joseph Davidovits in 1970s. It was first used as a fire resistant to protect cruise ships from fire, in protection of wooden structures and in different implementations. Geopolymers have also been shown to display good mechanical and thermal properties, low shrinkage and longer design lives compared to some cementitios materials. Geopolymers, if used as an alternative to Portland cement, CO_2 emission produced by geopolymer technology is estimated to be 80 % less than Portland cement. Therefore, it is thought that geopolymer technology is going to be vital in the near future for a green construction industry [9-11].

1.1. Geopolymerization Process

Geopolymer is an amorphous aluminosilicate structure formed by combining raw materials containg high levels of silica and alumina with alkali activating solutions [12-14] Geopolymer studies have started to increase in construction material field as geopolymer technology offers low CO_2 emission and low energy consumption. In addition, the resulting materials display good mechanical properties [12], acid resistance, freeze-thaw

cycle resistance, low permeability and the property of tendency to reducing the mobility of a great amount of heavy metal ions [15-18].

The general formula of three dimensional aluminosilicate geopolymer structure is $M_n[-(SiO_2)_z-AlO_2]_n.wH_2O$. M is a cation (Na, Ca, K), n is the polycondensation degree and z is 1, 2, 3 or >>3. This structure includes SiO_4 and AlO_4 tetrahedras linked by sharing all O atoms [19]. In geopolymerization process, aluminosilicates are usually used as raw materials and alkali hydroxide and silicate solutions are used to activate aluminosilicates. Reaction mechanisms are briefly shown below in Equation 1.1 and 1.2 [13].

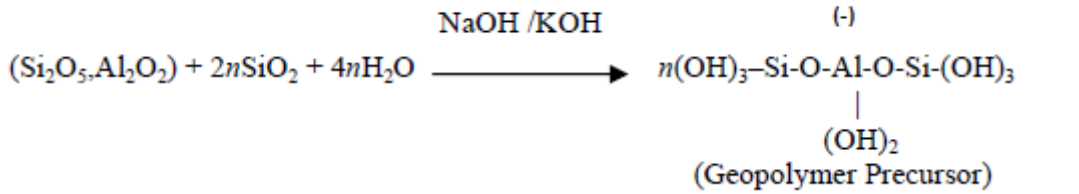

(1.1)

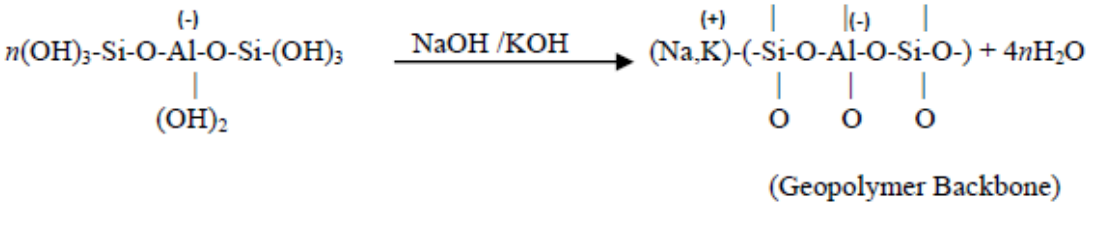

(1.2)

Formation of a geopolymer is a complicated process that can be summarized in mainly four steps:

(i) Dissolution of aluminosilicate solid materials in alkaline environment,

(ii) Geopolymer formation with the oxygen atoms in Si-O-Si and Si-O-Al bonds,

(iii) Partial precursors and polysilicate restructuring yield a 3D aluminosilicate framework, and

(iv) Unresolved solid molecules bond with each other [15, 20,21].

1.2. Raw Materials Used in Geopolymerization

Raw materials that can be used in geopolymerizatin as mentioned above are aluminosilicate sources that can be natural minerals including kaolinite and clays and industrial wastes such as fly ash, red mud, silica fume, rice-husk ash and slag [2].

Kaolinite is an aluminosilicate mineral used traditionally as a raw material in geopolymer synthesis due to its high content of SiO_2 and Al_2O_3. Turkey is an important kaolinite producer with a production capacity of about 850,000 metric tonnes annually [22]. Kaolinite displays a layered structure consisting of Al and Si layers with water molecules embedded in these layers. In geopolymer synthesis, thermally treated form of kaolinite, metakaolin, is used. Metakaolin can be obtained by calcination of kaolinite mineral at about 750 ºC [23]. In other words, dehydroxylation of kaolinite results in the formation of metakaolin. The process of dehydroxylation of kaolinite is seen in Figure 1.1. Metakaolin displays a relatively ordered structure consisting of layered silicon and aluminum layers [24]. The geopolymer formation process using metakaolin is expected to result in destruction of these layers leading to an amorphous geopolymer.

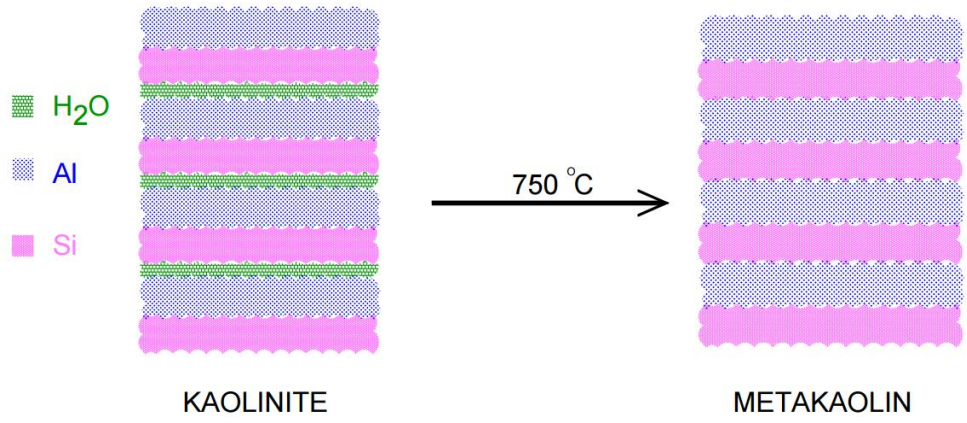

Figure 1.1. Dehydroxylation of kaolinite structure.

Fly ash is a subsidiary product obtained from the combustion of coal in thermal power plants [25]. It is suitable for geopolymer production due to its high amorphous silica and alumina content [26]. Composition of coal and the process of burning determine properties and chemical composition of fly ash [27,28]. According to ASTM C 618, fly ash is divided into two groups: class F and class C. They all have pozzolanic properties. However, in addition to this feature, C type fly ash also has some cementitious properties [29,30]. Lignite coal is a significant source for energy production in Turkey. Million tons of coal have been used for burning in thermal power plants annually and whereupon a great amount of fly ash and other combustion spin off products are produced in Turkey [31]. There are approximately 20 thermal power plants in Turkey. However C-type fly ash is produced by majority of them and F-type fly ash is produced only in Çatalağzı Thermal

Power Plant [27]. In general, F type fly ash contains low amount of CaO whereas C type fly ashes include up to 20 % CaO [27,32].

Another industrial waste used in geopolymer studies is red mud that is the main waste of aluminum production process [33,14]. More than 120 million tons of red mud is produced annually in the world [33,14]. Disposal method of red mud such as transportation to waste lakes, dewatering and drying is hazardous for environment and public health. Therefore, red mud treatment, recycling and utilization are enviromentally friendly actions. [33]. Using red mud in geopolymerization technology will contribute to evaluating huge mass of red mud waste in making an environmentally friendly material.

Approximate chemical compositions of fly ash, metakaolin and red mud are shown in Table 1.1. It is seen that metakaolin has less impurities compared to fly ash and red mud. These materials also differ in molar Si/Al ratio in their compositions. For example Si/Al ratio is about 2 in fly ash whereas it is about 1 in metakaolin.

XRD pattern of fly ash display a broad hump between 20 and 38^{o} indicating a dsordered structure. Generally fly ash contain some crystalline phases such as quartz (SiO_2), hematite (Fe_2O_3), anhydrite ($CaSO_4$), calcium oxide (CaO) and magnesioferrite ($MgFe_2O_4$) [34]. On the other hand, metakaolin displays a broad XRD pattern centered at about 27.5^{o} usually together with minor quartz content [35]. The main crystalline components in red mud are quartz (SiO_2), hematite (Fe_2O_3), goethite (FeO(OH)), and low amounts of sodalite ($Na_8(Al_6Si_6O_{24})Cl_2$) and cancrinite ($Na_6Ca_2Al_6Si_6O_{24}(CO_3)_2$) phases [36].

Table 1.1. Chemical compositions of metakaolin, F type and C type fly ash and red mud [36-38].

Component	Metakaolin	Fly ash F glass	C type fly ash	Red Mud
SiO_2	52.00	45.10	34.19	29.20
Al_2O_3	43.00	21.36	11.71	15.20
Fe_2O_3	2.00	4.81	9.93	31.50
K_2O	-	1.47	0.70	-
TiO_2	3.00	1.02	0.46	-
CaO	-	8.74	30.19	4.50
Na_2O	-	5.19	0.24	3.10
SO_3	-	5.19	3.38	-
MgO	-	3.49	7.11	0.20
MnO	-	0.09	1.11	-
LOI	-	3.54	0.32	10.20

1.3. Geopolymer Structure and Mechanical Properties

The structure and mechanical properties of geopolymers depend strongly on many factors including raw material selection, synthesis conditions, thermal treatment temperatures and durations following synthesis and etc.

X-ray diffraction (XRD) results show that metakaolin and fly ash based geopolymers are amorphous displaying a featureless hump in the XRD pattern. As the temperature increases, with increasing alkali activation with time, it might be expected to see crystalline phases in geopolymer structure [39]. For example in a metakaolin based amorphous geopolymer gel system, curing at different temperatures resulted in zeolite K-I phase formation at 120 ^{o}C. This result also proves that crystallinity increases as a function of temperature. On the other hand, as the polymerization degree of soluble silica is risen, more amorphous geopolymer gels form [39].

^{27}Al and ^{29}Si magic angle spinning (MAS) nuclear magnetic resonance (NMR) spectroscopy revealed that geopolymer structure consists of tetrahedrally coordinated Si^{4+} and Al^{3+} [39,40]. Typical metakaolin, metakaolin based Na geopolymer, typical fly ash and

fly ash based Na geopolymers have been characterized by ^{27}Al and ^{29}Si MAS NMR spectroscopy. It is reported that geopolymer structure is composed of crosslinked AlO_4 and SiO_4 tetrahedra, independent of raw material selection. ^{27}Al MAS NMR spectroscopy results indicate that the fundamental difference between fly ashes and metakaolin is that fly ashes include more Al than metakaolin [39].

FTIR spectra of geopolymers is generally characterized by a broad band in 900-1300 cm^{-1} region that is characteristic for disordered geopolymer structure. In a metakaolin based geopolymer study highest absorbance peak observed in the region 1300-900 cm^{-1} is assigned to asymmetric stretching vibration of Si-O-T linkages. The bands positioned at 1169 and 1063 cm^{-1} indicate the asymmetric stretching mode of metakaolin and these peaks were present in all spectra. The high frequency band at 995 cm^{-1} correponds to asymmetric vibration of oxygen linkages between tetrahedra of geopolymer structure [41]. In another study related to metakaolin-based geopolymers with different solid/liquid ratios, the main bands in FTIR spectra are observed at between 958 and 967 cm^{-1}. The band located at 660 cm^{-1} which is present in all geopolymer samples is related to the zeolite structure. The FTIR band positioned at 3300 cm^{-1} represents the OH stretching vibration. The other absorption peak at 1645 cm^{-1} is assigned to H_2O bending due to weak H_2O bonds adsorbed at the surface of the geopolymer framework [42]. FTIR spectra of kaolinite and fly ash based geopolymer indicates that the peaks positioned around 539 cm^{-1} are related to Si–O–Al bonds [20,43]. FTIR characteristic vibrations located at 1009 and 1033 cm^{-1} are due to the assymetric stretching of Al-O and Si-O bonds [20,44]. Another characteristic peak corresponds to asymetric stretching of linkages between tetrahedra was detected at 1087 cm^{-1} [20].

The mechanical properties of geopolymers is related with many factors including raw material selection, synthesis parameters and thermal treatment conditions following synthesis. For example, in a recent study in fly ash-based geopolymers, it is shown that as the thermal treatment temperature rises or aging time is extended, the strength of materials increases [45]. In another study, the maximum compressive strength for fly ash based geopolymer is observed when curing temperature is 60 ^oC. High curing temperature is observed to cause cracking. Moreover, the product including more Si than others has improved compressive strength with the values such as 64 MPa in this system [46].

Similarly, it is shown that metakaolin based geopolymers with higher Si/Al ratio does not display cracks and have minimum degradation [47]. A recent study in metakaolin-based geopolymer sytem focusing different curing temperatures within the range of 30 and 90 $^{\circ}$C, reported that 60 $^{\circ}$C was the optimum temperature for geopolymer samples in terms of showing good physical and mechanical properties [48]. Another research on metakaolin-based geopolymer specimens focused on changing Si/Al molar ratios in the system in the region of 1.07-1.90. It is observed that sample with Si/Al ratio of 1.75 has the best mechanical performance with the compressive strength value of 22 MPa [49].

The properties of fly ash and metakaolin based geopolymers are different than one another. First of all, fly ash based geopolymers tend to be stronger than metakaolin based geopolymers. These differences arise from their different microstructures. On the other hand, they have some similarities existing between them such as their local structures. They all have same gel phase binder and display same silicon and aluminium bonding environment at short length scales [39]. A study on metakaolin based geopolymers report that with increasing Si/Al ratio in the system, large pores decrease in size and conversion of heterogeneous structure into a homogeneous form takes place. It is observed that this change is proportional to increase in mechanical strength of geopolymers [50].

Various structural and mechanical testing methods are performed on red mud and fly ash based geopolymer systems with red mud contents between 0-40 percent. It is observed that the intensity of geopolymerization is enhanced as red mud composition in the system increased. Compressive strength values increase until 10 % red mud composition of geopolymer while further increase in red mud content resulted in a negative effect on compressive strength. Highest compressive strength values of geopolymer specimens are reported to be approximately about 20 MPa and 28 MPa for curing times 3 and 28 days, respectively [36]. In another study, red mud and granulated blast furnace slag are employed in geopolymerization. It is reported that geopolymer with red mud calcined at 800 $^{\circ}$C has the highest dissolution efficiencies of aluminium and silica. All produced binders are cured for 3, 7 and 28 days. It is found that geopolymer waited for 28 days exhibit the highest compressive strength value [51]. Mechanical performance of geopolymers produced with red mud and F type fly ash has been also studied recently as a function of molar composition. It is reported that Na/Al molar ratio in the range of 0.6-0.8

and Si/Al molar ratio of 2 are ideal beginning points to produce red mud and class F fly ash based geopolymers [12].

Understanding the structure of geopolymers is critical for designing geopolymers with desired properties. The relationships established between the structure and physical properties will be important for controlling product properties. In this context, this study includes synthesis, characterization, and modeling of metakaolin and fly ash&red mud based geopolymers for geopolymer design. In Chapter 2, metakaolin based geopolymer samples with different Si/Al ratios were synthesized, characterized and tested by some methods to understand microstructural and physical properties. In Chapter 3, C type fly ash based geopolymers with different Si/Al ratios and fly ash-red mud based geopolymer samples with different red mud composition were produced and characterization detail. X-ray diffraction (XRD), Fourier transform infrared spectroscopy (FTIR), Scanning electron microscopy (SEM) and compressive strength measurements were the main characterization methods employed in this thesis. XRD was performed on samples to detect crystalline phases and/or amorphous character of the specimens. FTIR analysis was carried out to determine the vibrational spectra of the samples. SEM images of all synthesized geopolymer samples were obtained to comprehend their characteristic structure. Furthermore, compressive strength analysis were performed on produced specimens to correlate microstructure and mechanical performance of geopolymer samples.

2. RELATIONS BETWEEN THE STRUCTURAL CHARACTERISTICS AND COMPRESSIVE STRENGTH IN METAKAOLIN BASED GEOPOLYMERS WITH DIFFERENT MOLAR SI/AL RATIOS

2.1. Introduction

Portland cement production is responsible for about 5-8 % of all human generated CO_2 emissions in the world. A tone of CO_2 is released for every ton of cement manufacture. It is a big environmental problem and the need for environmentally friendly construction materials is continuously growing. Recent research in geopolymer field showed that these new materials could be a potential alternative to Portland cement that could decrease CO_2 emission by 80 % compared to Portland cement [10,11,39,52]. Geopolymers are amorphous to crystalline alkali aluminosilicate materials formed by the reaction of an aluminosilicate source with alkali hydroxide and/or alkali silicate solution. Some other common terms used to refer geopolymers include 'low-temperature aluminosilicate glass', 'geocement', 'alkali-bonded ceramic', and 'hydroceramic' [39,53-56]. Geopolymers, when compared to traditional cementitious materials, have shown to display comparible physical and mechanical properties such as high compressive strength, significant acid and fire resistance, low thermal conductivity and low shrinkage [11,39]. Therefore they can be considered as potential future alternatives to cement-based materials.

Geopolymers can be thought as three-dimensional inorganic polymers that are produced by polymerization reaction of a solid aluminosilicate source with highly condensed alkali hydroxide or silicate solution [57,58]. Various aluminosilicate sources can be used as raw materials for geopolymer synthesis including kaolinite, fly ash and blast furnace slag [59]. The atomic structure and corresponding mechanical performance of the geopolymers depend strongly on the raw material employed in geopolymerization as well as the synthesis and aging conditions [39].

Metakaolin, thermally treated form of kaolinite mineral, has been widely used as the main raw material in geopolymerization in various studies before. Some recent studies involve utilization of metakaolin synergistically with industrial waste materials such as red mud, rice husk ash, and fly ash in geopolymerization [60,61,33,62,36]. Although the geopolymer formulations that exist in the literature seem to be promising in terms of achieving comparable mechanical performance values compared to cementitious materials, establishing structure-property relationships by through characterization of these materials will be critical for being able to design geopolymers with desired properties. In this context, this study, aims to synthesize and fully characterize metakaolin-based geopolymers with different Si/Al ratios in order to obtain relationships between the experimental structural characteristics and mechanical performance in geopolymer systems. Metakaolin is used as the main raw material in this study due to its high purity with respect to other aluminosilicate materials offering relatively easier data interpretation. The focus of this work is not optimization of geopolymer performance but to correlate geopolymer performance with the structural data that is collected on metakaolin-based geopolymers with various Si/Al molar ratios. Previous studies indicated that geopolymer formulations achieved high compressive strength values for molar Si/Al and Na/Al ratios in the regions 1.8-2.2 and 0.9-1.2, respectively [58,63-65]. In order to complement these kinds of conclusions, the structural characteristics in the geopolymer systems should be outlined employing various structural characterization techniques in order to understand the mechanical behavior of a system. In this study, X-ray diffraction (XRD), Fourier Transform Infrared Spectroscopy (FTIR) and scanning electron microscopy (SEM) are synergistically employed to understand structural characteristics of metakaolin-based geopolymers. Compressive strength measurements are performed on the synthesized materials to correlate mechanical performance of these materials with their structural characteristics.

2.2. Experimental

Kaolinite was treated at 700 ^{o}C at atmospheric pressure for 1 hour to obtain metakaolin. Metakaolin is known to be more active for geopolymerization and was used as the aluminosilicate source to produce geopolymers in this study. Metakaolin was allowed

to rest about a day before being used in geopolymerization. Chemical composition of metakaolin used in this study is given in Table 2.1.

Table 2.1. Chemical composition (wt %) of metakaolin.

Chemical Composition	**Percentage (wt %)**
SiO_2	56.21
Al_2O_3	41.04
TiO_2	1.15
K_2O	0.46
Fe_2O_3	0.36
CaO	0.09
MgO	0.07
P_2O_5	0.06

Sodium hydroxide (NaOH) and sodium silicate (9 % of Na_2O, 28 % of SiO_2, 63 % of H_2O with 1.401 g/ml of density at 20 ^oC) solutions were used as activating solutions to form metakaolin-based geopolymers. Metakaolin and activating solutions are mixed thoroughly and transferred into 4 cm x 4 cm x 16 cm steel molds using the described conditions in Table 2.2.

Table 2.2. Synthesis conditions and molar ratios used in metakaolin-based geopolymer synthesis. Geopolymer (GP) samples were named using the Si/Al molar ratio and the time (days) the samples were cured at 60 °C. For instance, GP1.12-7d refers to geopolymer formulation with Si/Al ratio of 1.12 that was cured at 60 °C for 7 days and three weeks.

Geopolymer	**Si/Al**	**Na/Al**	**Na/Si**	**Activating Solution**	**Solid to water ratio (g/g)**	**Thermal Treatment**
GP1.12-1d	1.20	1.492	1.280	NaOH	1.05	1 day-60 ^{o}C + 3 weeks-25 ^{o}C
GP1.12-7d	1.20	1.492	1.280	NaOH	1.05	7 days-60 ^{o}C + 3 weeks-25 ^{o}C
GP1.77-1d	1.80	1.123	0.635	NaOH & $Na_2Si_3O_7$	1.19	1 day-60 ^{o}C + 3 weeks-25 ^{o}C
GP1.77-7d	1.80	1.123	0.635	NaOH & $Na_2Si_3O_7$	1.19	7 days-60 ^{o}C + 3 weeks-25 ^{o}C
GP2.20-1d	2.20	1.193	0.542	NaOH & $Na_2Si_3O_7$	1.12	1 day-60 ^{o}C + 3 weeks-25 ^{o}C
GP2.20-7d	2.20	1.193	0.542	NaOH & $Na_2Si_3O_7$	1.12	7 days-60 ^{o}C + 3 weeks-25 ^{o}C

They were allowed to rest about a few hours before being transferred into furnace. GP1.12-1d and GP1.12-7d were produced using 8M NaOH solution to activate metakaolin whereas the other geopolymers were produced using $Na_2Si_3O_7$ solutions together with 8M NaOH solution to achieve higher molar Si/Al ratios. Sodium silicate ($Na_2Si_3O_7$) solution contains soluble SiO_2 facilitating synthesis of geopolymers with Si/Al ratios of 1.77 and 2.20 (GP1.77-1d, GP1.77-7d, GP2.20-1d and GP2.20-7d). Geopolymer samples in this study were synthesized with molar Si/Al ratios of 1.12, 1.77 and 2.20. As a part of this study, it was also aimed to see the changes in structure and mechanical performance with exposure to different thermal treatments as well as molar Si/Al ratios. Therefore, each geopolymer composition was treated through two different thermal procedures to see the effect of thermal processing history. The samples with different Si/Al ratios, following mixing process, were cured i) 1 day at 60 ^oC and 3 weeks at 25 ^oC, and ii) 7 days 60 ^oC and 3 weeks at 25 ^oC. All experimental measurements were performed on these samples at the end of mentioned curing times.

All obtained specimens are characterized by XRD (absorber: copper, model: D/Max 2200-PC, Rigaku) to determine crystalline phases and/or amorphous character of the specimens. Powder XRD patterns were recorded on a Rigaku X-ray diffractometer (model: D/Max 2200-PC) with Cu absorber. FTIR spectroscopy (Bruker Vertex 80v spectrometer, resolution: 4 cm^{-1}) analysis in 2000-400 cm^{-1} spectral region were performed on produced geopolymer samples to determine the vibrational spectra of the samples. Compressive strength measurements were performed by a servo-hydraulic test machine with capacity of 100 kN (model: MTS) and loading rate is 0.01 mm per second. SEM images were obtained by using Zeiss Ultra Plus (FEG-SEM) scanning electron microscope with a secondary electron (SE) detector.

2.3. Results and Discussions

Metakaolin was obtained by thermal treatment of kaolinite at 700 ^oC for an hour. Figure 2.1 displays XRD patterns of kaolinite and metakaolin. Distinct characteristic features in the XRD pattern of kaolinite disappeared as a result of thermal treatment at 700 ^oC resulting in a broad feature that is located between 2θ of 20-28° indicating loss of crystallinity and order in the system (Figure 2.1). This process is an indication of

dehydroxylation process of kaolinite by loss of structural water through diffusion followed by transformation of six-coordinated aluminium into four-fold [66]. It was observed that both kaolinite and metakaolin included quartz as a minor impurity (Figure 2.1).

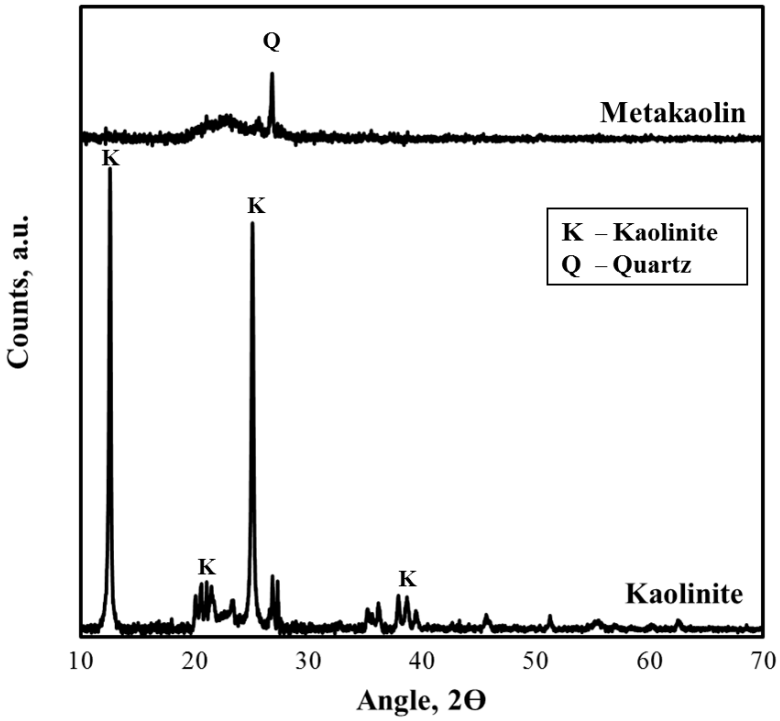

Figure 2.1. XRD patterns of kaolinite and metakaolin.

FTIR spectra of kaolinite and metakaolin are given in Figure 2.2. The band positioned at 1116 cm^{-1} is attributed to Si-O stretching vibrations in kaolinite structure. A significant band at 1029 cm^{-1} and a major shoulder at 1014 cm^{-1} are assigned to Si-O-Si and Si-O-Al lattice vibrations in kaolinite, respectively [67,68]. Sharp bands located at 941 and 919 cm^{-1} in the FTIR spectrum indicate surface OH bending and inner OH bending vibrations that are mainly caused by Al-OH groups, respectively (Figure 2.2) [67,69]. Bands in the low frequency region positioned at 759, 694 and 536 cm^{-1} are related with Si-O and Al-O vibrations [67,68]. Specifically, the band centered at 536 cm^{-1} corresponds to Al $(O,OH)_6$ octahedra in kaolinite [67,70]. Another lower frequency band at 464 cm^{-1} is attributed to bending or stretching of T-O-T (T=Si or Al) bridge of aluminosilicates [71,72]. Thermal treatment of kaolinite at 700 °C results in transformation of crystalline kaolinite into amorphous metakaolin with the loss of internal water and dehydroxylation as

it is evident from Figure 2.1. In this context, the characteristic bands observed in the FTIR spectrum of kaolinite disappeared and broad features positioned around 1080, 808 and 465 cm^{-1} appeared (Figure 2.2). High frequency band at 1080 cm^{-1} is attributed to stretching Si-O bonds in amorphous SiO_2.

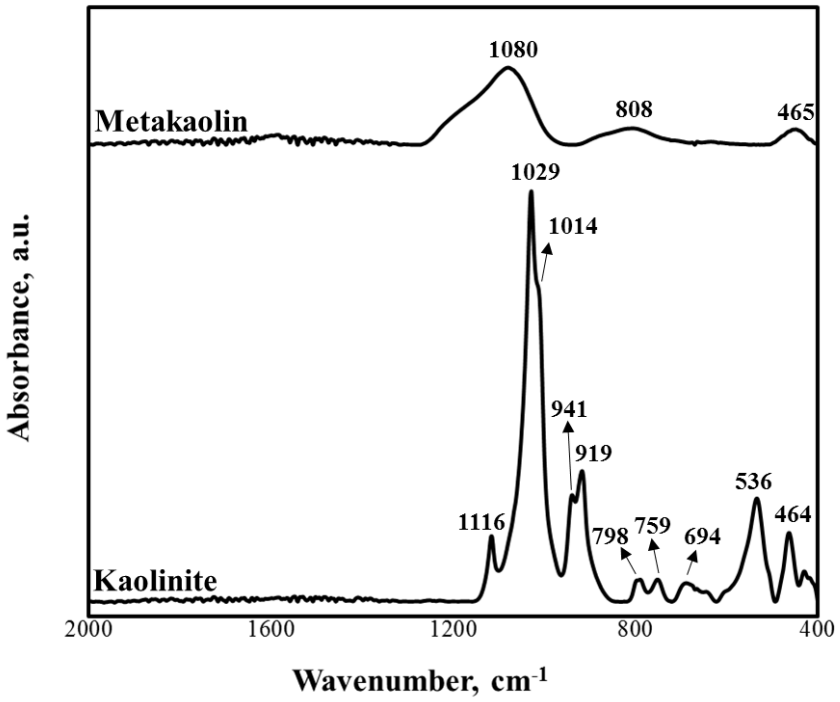

Figure 2.2. FTIR spectra of kaolinite and metakaolin.

Low frequency band positioned at 536 cm^{-1} in kaolinite is replaced by a broad band at 808 cm^{-1} which is related to the vibrations of the AlO_4 tetrahedron in metakaolin [70,72]. FTIR band located at 464 cm^{-1} in the FTIR spectrum of kaolinite indicating T-O-T (T: Si or Al) aluminosilicate bridge is seen in the FTIR spectrum of metakaolin as well displaying a broader peak compared to kaolinite.

In this study metakaolin was activated to form geopolymers with molar Si/Al ratios between 1.12-2.20. XRD patterns of all geopolymers studied in this work are given in Figure 2.3. It can be seen from this figure that, the specimen with Si/Al ratio of 1.12 with thermal curing of 1 day at 60 °C and three weeks at room temperature (GP1.12-1d) consists of mainly zeolite A and minor amount of sodalite phases. On the other hand, GP1.12-7d sample that corresponds to same molar Si/Al ratio with longer treatment at

60 °C seems to be comprised of mainly sodalite (Figure 2.3). XRD patterns of geopolymers with Si/Al molar ratio of 1.77 and 2.20 (GP1.77-1d, GP1.77-7d, GP2.20-1d and GP2.20-7d) all display a featureless hump centered at approximately 27-29^{o} 2θ that indicate the formation of an X-ray amorphous geopolymer matrix [39]. These geopolymers seem to contain quartz in their structures as well (Figure 2.3). SEM images of these samples are given in Figure 2.4 and they seem to support XRD results.

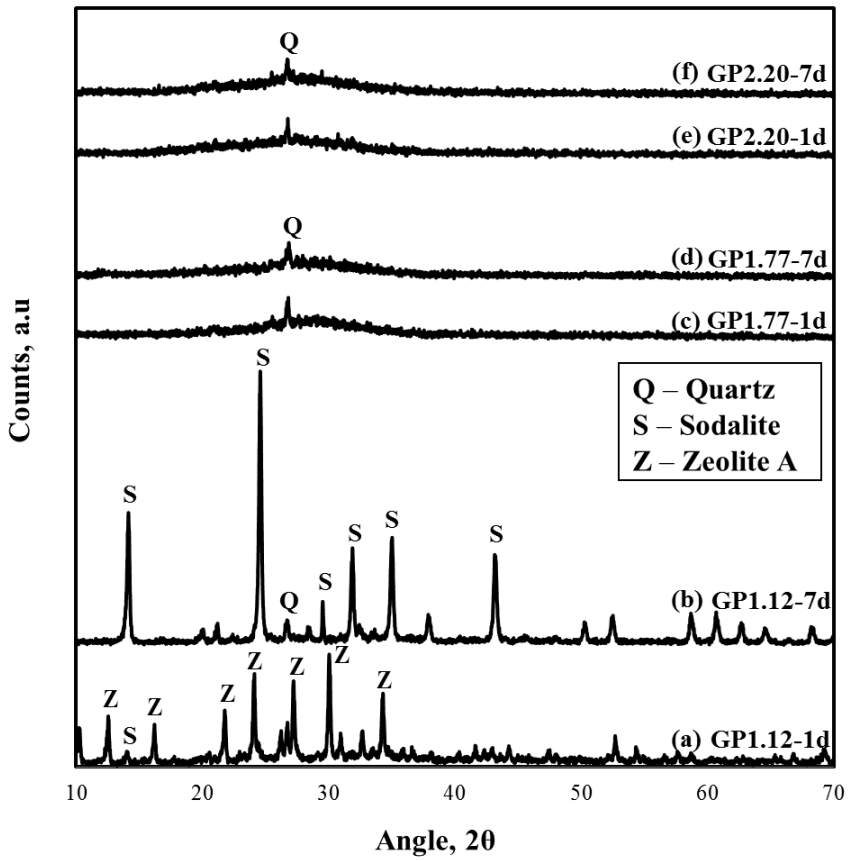

Figure 2.3. XRD patterns of geopolymers **(a)** GP1.12-1d (Si/Al ratio: 1.12), **(b)** GP1.12-7d (Si/Al ratio: 1.12), **(c)** GP1.77-1d (molar Si/Al ratio: 1.77), **(d)** GP1.77-7d (Si/Al ratio: 1.77), **(e)** GP2.20-1d (Si/Al ratio: 2.20), **(f)** GP2.20-7d (Si/Al ratio: 2.20).

The morphology of specimen GP1.12-1d displays cubic zeolite A crystals that are also detected by XRD. The sizes of these cubes seem to be about 1 μm and interpenetration twinning is observed consistent with the literature [67]. On the other hand, specimen GP1.12-7d displays the presence of wedge-shaped blade morphology that is consistent with sodalite formation in the system. As it is seen in Figure 2.4, the SEM morphologies

for specimens with higher Si/Al molar ratios (GP1.77-1d, GP1.77-7d, GP2.20-1d and GP2.20-7d) display glassy geopolymeric matrices, consistent with their x-ray amorphous XRD patterns (Figure 2.4).

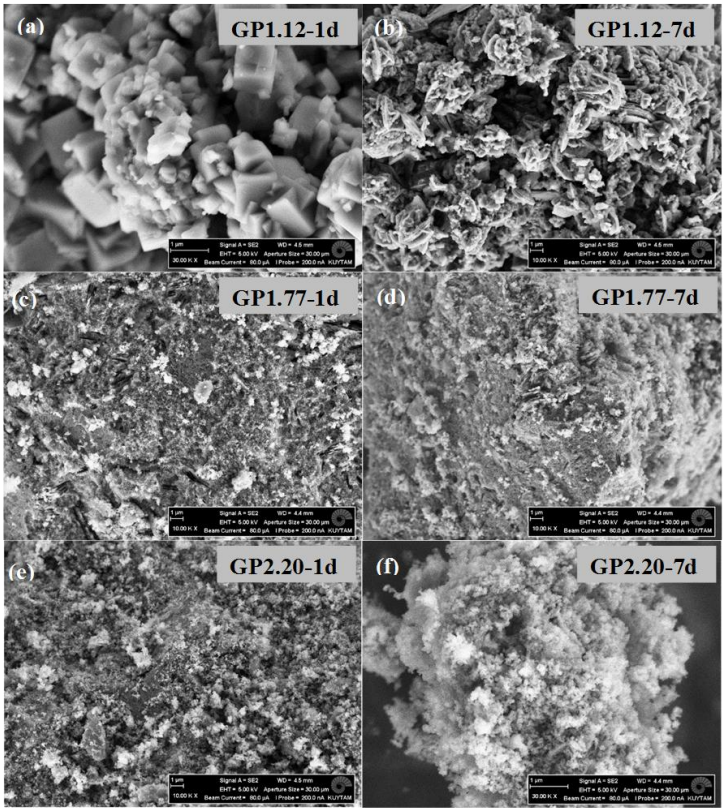

Figure 2.4. SEM images displaying morphology of geopolymers **(a)** GP1.12-1d (Si/Al ratio: 1.12), **(b)** GP1.12-7d (Si/Al ratio: 1.12), **(c)** GP1.77-1d (Si/Al ratio: 1.77), **(d)** GP1.77-7d (Si/Al ratio: 1.77), **(e)** GP2.20-1d (Si/Al ratio: 2.20), **(f)** GP2.20-7d (Si/Al ratio: 2.20).

FTIR spectra of the geopolymers studied in this work are shown in Figure 2.5. A visual inspection of Figure 2.5 shows that geopolymers with molar Si/Al ratio of 1.12 (GP1.12-1d and GP1.12-7d) exhibit much narrower FTIR band widths. This fact is consistent with relatively high level of crystallinity in these samples as indicated from XRD patterns in Figure 2.3. On the other hand, geopolymers with molar Si/Al of 1.77 and 2.20 that display 'x-ray amorphous' XRD patterns (GP1.77-1d, GP1.77-7d, GP2.20-1d and GP2.20-7d) exhibit fairly broad main bands in their FTIR spectra. It is observed that the main band positioned at about 1085 cm^{-1} in the FTIR spectrum of metakaolin (Figure 2.2)

is replaced by bands in the lower frequecy region (950-1150 cm^{-1}) as a result of geopolymerization reaction of metakaolin with activating solutions (Figure 2.5). XRD results for the geopolymers with Si/Al ratio of 1.12 indicated that GP1.12-1d consisted of mainly zeolite A with minor sodalite component whereas GP1.12-7d contained mainly sodalite phase. Therefore, increased curing time at 60 °C resulted in the formation of sodalite phase. This result obtained from diffraction is verified by FTIR spectroscopy. FTIR spectrum of GP1.12-1d exhibits a major band located at 977 cm^{-1} which is assigned to Si-O-Al bonds in TO_4 tetrahedra in zeolites [72,73]. Moreover the band positioned at around 555 cm^{-1} is a characteristic feature attributed to the formation of double four-membered rings in zeolite structure [72,74]. On the other hand, the FTIR spectrum of GP1.12-7d as shown in Figure 2.5 reveals characteristic bands that are fingerprints of natural sodalite minerals, supporting XRD findings in Figure 2.3. Specifically, the main band at around 966 cm^{-1} can be attributed to asymmetric stretching mode of T-O-T bonds. The features located at 734, 711 and 667 cm^{-1} are characteristic symmetric stretching vibrations of T-O-T bonds in sodalite framework [67,69]. The bands positioned at 462 cm^{-1} and 430 cm^{-1} in the lower frequency region are related to the bending of O-T-O bonds in GP1.12-7d (Figure 2.5) [67].

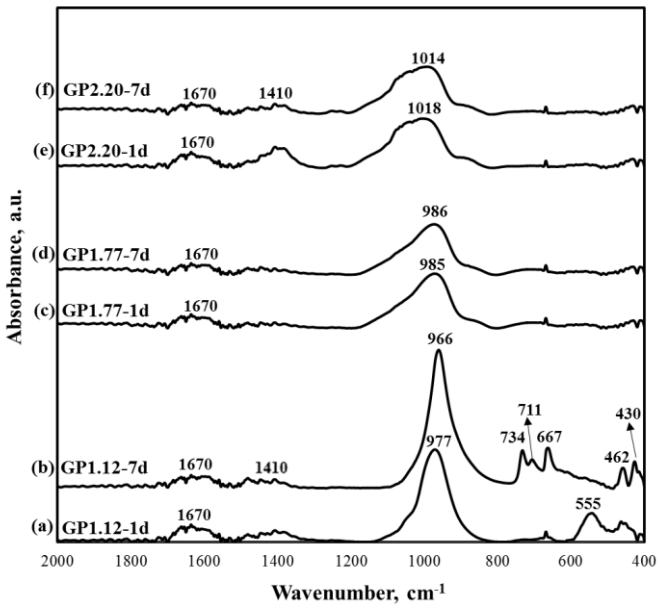

Figure 2.5. FTIR spectra of geopolymers **(a)** GP1.12-1d (Si/Al ratio: 1.12), **(b)** GP1.12-7d (Si/Al ratio: 1.12), **(c)** GP1.77-1d (Si/Al ratio: 1.77), **(d)** GP1.77-7d (Si/Al ratio: 1.77), **(e)** GP2.20-1d (Si/Al ratio: 2.20), **(f)** GP2.20-7d (Si/Al ratio: 2.20).

FTIR spectra of geopolymers with molar Si/Al ratios of 1.77 and 2.20 are characterized by the presence of a fairly broad 'main band' in the region 900-1200 cm^{-1}. As it can be seen from Figure 2.5, geopolymers with Si/Al molar ratio of 1.77 (GP1.77-1d and GP1.77-7d) display broad main bands at around 985 cm^{-1}. However, main bands in the FTIR spectra of geopolymers with Si/Al molar ratio of 2.20 (GP2.20-1d and GP2.20-7d) seem to be positioned at a higher frequency of 1014-1018 cm^{-1}. Main band in the FTIR spectrum is a major indication of inorganic polymeric matrix defining asymmetric stretching vibrations of T-O-Si (T: Si or Al) bonds as a result of TO_4 reorganization during geopolymer synthesis [75,76]. This band was reported to depend on the length as well as angle of the bonds in the structure. The intensity of this band was also indicated to decrease with increased Al incorporation into geopolymer matrix [75,76]. In this study, the main band position in the FTIR spectra is observed to systematically shift to higher wavenumbers with increasing molar Si/Al ratio with increased peak widths. In addition, the intensity of the main band decreased with increasing Si content in the system (Figure 2.5). This is attributed to increased geopolymerization and disorder in the system. It should also be noted that the band located at 1670 cm^{-1} is related to bending vibrations of H-O-H [51] and the intensity of this peak slightly decreases with increased thermal treatment times at 60 °C. Specimens GP2.2-1d and GP1.12-1d display a broad feature at 1410 cm^{-1} in their FTIR spectra that can be assigned to stretching vibrations of O-C-O bond indicating atmospheric carbonation. Excess sodium in the geopolymer matrix might have reacted with CO_2 to result in sodium bicarbonate [75,77].

Figure 2.6 displays compressive strength values measured for the geopolymer samples investigated in this study as a function of molar Si/Al ratios in the structures. It is seen that the specimens with the lowest molar Si/Al ratio of 1.12 display very low compressive strength values of about 1 MPa as expected from their somewhat crystalline nature. Compressive strength values seem to systematically increase with increasing Si content in the system (Figure 2.6). Previous studies indicated that increase in SiO_2 content in geopolymers by addition of soluble SiO_2 to the activating solutions can substantially reduce the level of long-range structural ordering [3]. In this work Si/Al ratios were controlled by adding sodium silicate solution (including soluble silica) to the system as well.

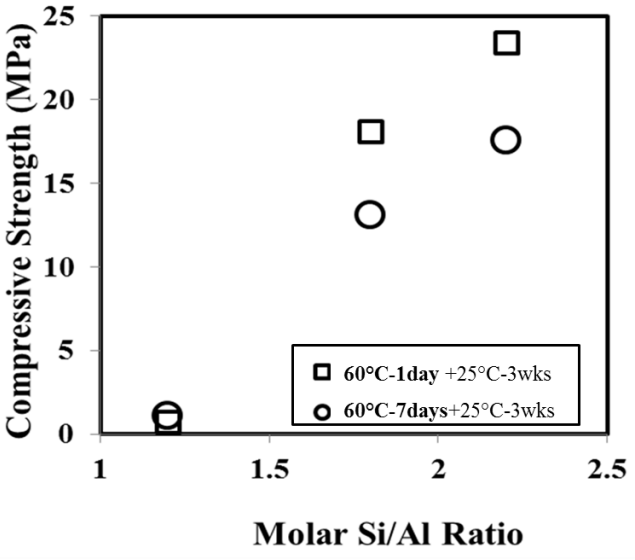

Figure 2.6. Compressive strength of the geopolymers as a function of molar Si/Al ratios.

This helped to obtain disordered geopolymer structures (specimens with Si/Al ratios of 1.77 and 2.20) as revealed from their XRD, FTIR and SEM results which in turn resulted in improved compressive strengths (13-23 MPa).

The geopolymer with molar Si/Al ratio of 2.2 that was cured shorter (1 day) at 60 °C (GP2.20-1d) exhibits the highest compressive strength of 23 MPa among the specimens studied here. Geopolymers that were treated for 1 day at 60 °C were observed to consistently have higher compressive strength values than specimens cured at 60 °C for 7 days (Figure 2.6). Longer exposure to higher temperature (60 °C) was seen to have a negative effect in the development of compressive strength. More exposure (7 days) to thermal treatment at 60 °C seemed to significantly decrease compressive strength values by about 5 MPa with respect to samples treated at 60 °C for 1 day. Previous studies in the literature regarding optimization of compressive strength in geopolymers indicated that metakaolin based geopolymers with molar Si/Al and Na/Al ratios in the regions of 1.8-2.2 and 0.9-1.2, respectively, attain maximum compressive strength values [8,15-17]. The results of this work also support these previous findings.

For specimens with molar Si/Al ratio of 1.12, the SiO_2 content in the system is much lower than the desired content for an optimum geopolymer. XRD patterns of these specimens displayed crystalline components namely zeolite A and/or sodalite phases which

are responsible for corresponding low compressive strength values of about 1 MPa (Figures 2.3 and 2.6). Crystalline nature of these specimens is also evident in their corresponding SEM images (Figure 2.4). On the other hand, geopolymers with Si/Al ratios of 1.77 and 2.20 (GP1.77-1d, GP1.77-7d, GP2.20-1d and GP2.20-7d) seem to fall in the region of an optimum geopolymer in terms of molar Si/Al and Na/Si ratios [8,15-17] and the corresponding compressive strength values of these samples were found to be significantly higher.

As discussed above, the features of the main bands in the FTIR spectra of the geopolymer specimens were also observed to exhibit systematic trends with increasing Si/Al molar ratio (Figure 2.5). These trends are consistent with the evolution of compressive strength in these materials. Figure 2.7 displays the position of the main FTIR band as a function of Si/Al ratio for specimens with different thermal histories. It can be seen that the position of the main band in FTIR spectra constantly shifts to higher frequencies with increasing Si content in the system, possibly indicating increased geopolymerization in the system (Figures 2.5 and 2.7). In addition, the main band in the FTIR spectra of specimens with thermal history of 1 day at 60 °C seem to be located at higher wave numbers compared to specimens with thermal history of 7 days at 60 °C. It is also seen in Figure 2.5 that the width of the main FTIR band increases significantly with increasing Si/Al ratio. Increased Si content in the geopolymer system was observed to result in x-ray amorphous structure that displays a fairly broad FTIR main band that is located at higher wave numbers. Therefore, it is observed that the system investigated in this work have a crystalline nature at Si/Al ratio of 1.12 whereas increase in Si/Al ratio resulted in the formation of a three dimensional geopolymeric network that display wider FTIR bands positioned at higher frequencies. These characteristics are highly correlated with the evolution of compressive strength in metakaolin-based geopolymers.

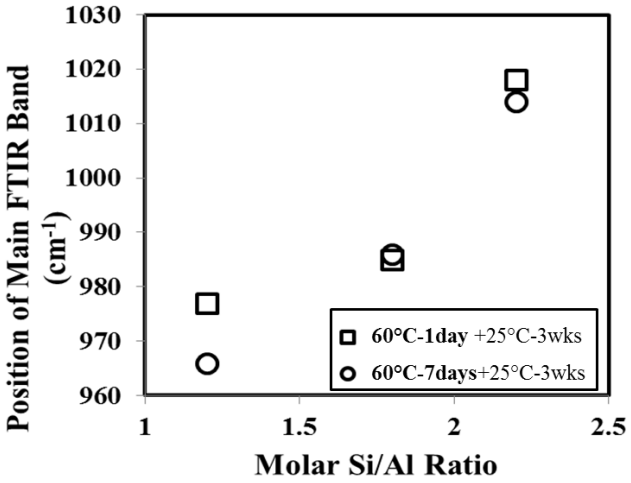

Figure 2.7. The positions of the main FTIR bands in geopolymers (based on Figure 2.5) as a function of molar Si/Al ratios.

2.4. Conclusions

Metakaolin-based geopolymers with molar Si/Al ratios of 1.12, 1.77 and 2.20 were synthesized and characterized by XRD, FTIR spectroscopy, and SEM. Compressive strength measurements were also performed on the corresponding samples. It was observed that samples with Si/Al ratio of 1.12 contained crystalline components, namely zeolite A and/or sodalite. These samples were observed to be rather brittle due to their highly crystalline nature with compressive strength values of around 1 MPa. Geopolymers with molar Si/Al ratios of 1.77 and 2.20 revealed amorphous XRD patterns and glassy SEM microstructures.

Main band in the FTIR spectra of these geopolymers in the region of 900-1200 cm^{-1} is indicative of geopolymerization and it systematically moved to higher frequencies with increasing molar Si/Al ratio. Evolution of this band is thought to be strongly correlated with the corresponding increases in the compressive strength of these materials.

3. RELATIONS BETWEEN THE STRUCTURAL CHARACTERISTICS AND COMPRESSIVE STRENGTH IN FLY ASH AND RED MUD- FLY ASH BASED GEOPOLYMERS

3.1. Introduction

Portland cement production causes greenhouse gas emissions [78,79]. On the other hand, geopolymers arise as environmentally friendly future alternatives to cement-based materials as they can be synthesized at fairly mild conditions with low energy costs. These materials are tempting as they display excellent properties such as low shrinkage, acid resistance and high mechanical strength [80,57,81,82]. Geopolymerization process involves alkali activation of a raw material including high amounts of silicon (Si) and aluminum (Al) by an alkali hydroxide and/or alkali silicate solution. A variety of raw materials such as fly ash, slags, rice husk ash, red mud, metakaolin and clays can be employed [80,10]. Sodium hydroxide (NaOH) is mostly used as a part of activating solution to activate raw materials due to the fact that dissolution of Al^{3+} and Si^{4+} ions can be easier in sodium hydroxide solution than potassium hydroxide solution [83-85]. Additionally, using sodium silicate solution has been shown to help producing geopolymers with good mechanical properties.

In this part of the thesis, the employment of two industrial wastes, fly ash and red mud, in geopolymerization is going to be investigated. Fly ash is an industrial waste obtained from the coal combustion in thermal power plants produced about 750 million tonnes in the world annually [38,86]. It can be classified based on its calcium content: C type fly ash refers to compositions with Ca> 20 % by weight and F fly ash refers to compositions including Ca< 20 % by weight [12,87]. There are numerous studies in geopolymer literature employing Class F fly ash in geopolymerization [12,87,45,46]. However, although produced in huge amounts annually, number of studies regarding utilization of C type fly ash in geopolymerization is rather rare. C type fly high calcium fly ash also includes silica and alumina. Therefore, Class C fly ash contains considerable amount of aluminosilicates in its structure; therefore its potential for utilization in

geopolymerization a raw material should be investigated in detail [78]. On the other hand, red mud is a spin off product of Bayer process of aluminium manufacture. 1.5-1.6 tons red mud are obtained from every ton of aluminium production [36,88]. Red mud includes aluminium (Al), silicon (Si) and iron (Fe) oxides and hydroxides that is used with some materials having high amounts of Si and Al in geopolymer synthesis [36,89,12]. In this study, high calcium lignite fly ash (C type) and red mud were used as raw materials in geopolymerization.

The main objectives of this part of the thesis are:

- to synthesize fly ash-based geopolymers with varying molar Si/Al ratios within the range of 1.95-2.40,
- to synthesize red mud and fly ash-based geopolymers with varying red mud contents, and
- to perform detailed structural characterization on these materials employing X-ray diffraction (XRD), Fourier Transform Infrared Spectroscopy (FTIR) and scanning electron microscopy (SEM)
- to correlate these structural characteristics with the results of compressive strength measurements performed on these geopolymers.

3.2. Experimental

In this study, fly ash and red mud based geopolymers are produced. Fly ash (FA) and red mud (RM) are obtained from Yatağan Thermal Power Plant and Seydişehir Eti Aluminium Plant respectively. Red mud was calcined at 800 ^{o}C for 3 h by thermal treatment in an ash furnace (Model: MT1210-B2, MagmaTherm). After calcination, red mud is treated at 100 ^{o}C for 3 hour. Chemical compositions of fly ash and red mud used in this study are given in Table 3.1.

Table 3.1. Chemical composition (wt %) of fly ash and red mud.

Compound	Fly Ash	Red Mud
SiO_2	34.04	12.59
Al_2O_3	14.89	16.85
CaO	26.32	1.44
Fe_2O_3	6.78	37.45
SO_3	12.23	0.25
K_2O	1.93	0.31
MgO	1.90	0.20
Na_2O	0.43	10.55
TiO_2	0.79	5.94
P_2O_5	0.19	-

Sodium hydroxide (NaOH) and sodium silicate (9 % of Na_2O, 28 % of SiO_2, 63 % of H_2O with 1.401 g/ml of density at 20 ^oC) solutions were used to activate red mud and high calcium fly ash in this study.

Two experiment sets were performed to produce geopolymers. In the first experiment set, only fly ash is used as the raw material. NaOH and sodium silicate solutions were used as activators to obtain geopolymer samples with different Si/Al molar ratios of 1.95, 2.10, 2.25 and 2.40. Alkali-activated samples are poured into 4 cm x 4 cm x 16 cm iron molds using the described experimental conditions in Table 3.2.

Table 3.2. Synthesis conditions and molar ratios used in fly ash-based geopolymer synthesis. Geopolymer (GP) samples were named using the Si/Al molar ratio and the time (days) the samples were cured at 60°C. For instance, GP2.10 refers to geopolymer formulation with Si/Al ratio of 2.10 that was cured at 60 °C for 1 days and four weeks.

Geopolymer	**Si/Al**	**Al/Na**	**Na/Si**	**Ca/Si**	**Ca/Al**	**Solid to water ratio (g/g)**	**Thermal treatment**
GP1.95	1.95	0.83	0.62	0.82	1.60	1.25	1 day-60 ^{o}C + 4 weeks-25 ^{o}C
GP2.10	2.10	0.83	0.57	0.76	1.60	1.25	1 day-60 ^{o}C + 4 weeks-25 ^{o}C
GP2.25	2.25	0.83	0.53	0.71	1.60	1.25	1 day-60 ^{o}C + 4 weeks-25 ^{o}C
GP2.40	2.40	0.83	0.50	0.67	1.60	1.25	1 day-60 ^{o}C + 4 weeks-25 ^{o}C

In the second experiment set, fly ash and red mud based geopolymer samples were prepared including 0, 10, 20, 30, 40 and 50 % red mud in the raw material mixture. Sodium silicate and NaOH solutions were mixed to prepare the activating solutions that were allowed to rest for 24 hours at room temperature. Obtained geopolymer gels were transferred into 4 cm x 4 cm x 16 cm iron molds using the described experimental conditions in Table 3.3. They allowed to rest a day before being transferred into furnace. In this part of study, it was intended to see the changes in structure and mechanical performance as a function of different red mud content in these geopolymers.

Table 3.3. Synthesis conditions and molar ratios used in fly ash-red mud based geopolymer synthesis. Geopolymer (GP) samples were named using the red mud composition. For instance, GP-RM10 refers to geopolymer formulation with red mud composition of % 10 that was cured at 60 °C for 1 days and four weeks.

Geopolymer	**Composition**	**Si/Al**	**Al/Na**	**Na/Si**	**Ca/Si**	**Ca/Al**	**Solid to water ratio (g/g)**	**Thermal treatment**
GP-RM0	0 % RM	2.00	0.83	0.60	0.80	1.60	1.25	1 day-60^{o}C + 4 weeks-25^{o}C
GP-RM10	10 % RM	2.00	0.83	0.60	0.71	1.43	1.25	1 day-60^{o}C + 4 weeks-25^{o}C
GP-RM20	20 % RM	2.00	0.83	0.60	0.63	1.27	1.25	1 day-60^{o}C + 4 weeks-25^{o}C
GP-RM30	30 % RM	2.00	0.83	0.60	0.55	1.10	1.25	1 day-60^{o}C + 4 weeks-25^{o}C
GP-RM40	40 % RM	2.00	0.83	0.60	0.47	0.95	1.25	1 day-60^{o}C + 4 weeks-25^{o}C
GP-RM50	50 % RM	2.00	0.83	0.60	0.39	0.79	1.25	1 day-60^{o}C + 4 weeks-25^{o}C

All produced samples were cured at 60 ^{o}C for 1 day and at 25 ^{o}C for 4 weeks. All experimental measurements were performed on geopolymer samples at the end of this period.

All obtained specimens were characterized by XRD (absorber: copper, model:D/Max 2200-PC, Rigaku) in order to determine the crystalline phases that were present in the system. Powder XRD patterns were recorded on a Rigaku X-ray diffractometer (model:D/Max 2200-PC) with Cu absorber. FTIR spectroscopy (Vertex 80v spectrometer, resolution: 4 cm^{-1}, Bruker) analysis at 2000-400 cm^{-1} spectral region were performed on produced geopolymer samples to determine the vibrational spectra of the samples. Compressive strength measurements were performed by a servo-hydraulic test machine with capacity of 100 kN (model:MTS) and loading rate is 0.01 mm per second. SEM images were obtained by using Zeiss Ultra Plus (FEG-SEM) scanning electron microscope with a secondary electron (SE) detector.

3.3. Results and Discussions

3.3.1. Fly Ash-Based Geopolymers With Molar Si/Al Ratios Between 1.95-2.40

XRD patterns of fly ash and fly ash-based geopolymer samples with molar Si/Al ratios of 1.95, 2.10, 2.25 and 2.40 is given in Figure 3.1. Lime, anhydrite and quartz seem to be the dominating crystalline phase in fly ash. By alkali activation of fly ash the diffraction pattern evolved into a different form. Anhydrite and lime phases disappeared and the formation of calcium hydroxide ($Ca(OH)_2$) and calcium carbonate ($CaCO_3$) phases were observed on specimens with Si/Al ratio of 1.95 and 2.10 and 2.25 and 2.40, respectively. A common broad feature of all samples that is located at about 2θ of 29° indicates the loss of crystallinity and formation of an amorphous phase within system (Figure 3.1).

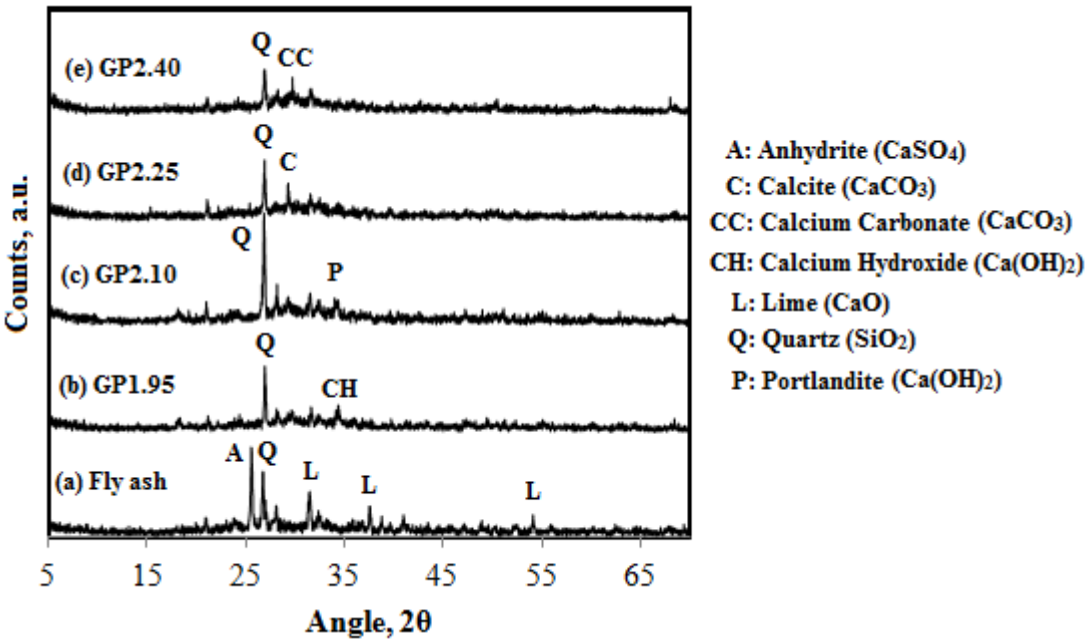

Figure 3.1. XRD patterns of C type fly ash and fly ash based geopolymers **(a)** Fly ash, **(b)** GP1.95 (Si/Al ratio: 1.95), **(c)** GP2.10 (Si/Al ratio: 2.10), **(d)** GP2.25 (Si/Al ratio: 2.25), **(e)** GP2.40 (Si/Al ratio: 2.40).

FTIR spectra of fly ash and fly ash based geopolymers with different Si/Al molar ratios are displayed in Figure 3.2. As it is evident from FTIR spectrum of fly ash, the low frequency bands seen at 592, 610 and 668 cm^{-1} are related to anhydrite presence in the structure [90]. This fact is also consistent with the results of XRD (Figure 3.1). A broad band located around 890 cm^{-1} could be related to C-O vibrations [91]. The FTIR spectrum of fly ash is dominated by an intense feature positioned at about 1100 cm^{-1}. This feature should be related to the asymmetric stretching vibrations of Si-O-Si and Al-O-Si in the structure [92-95].

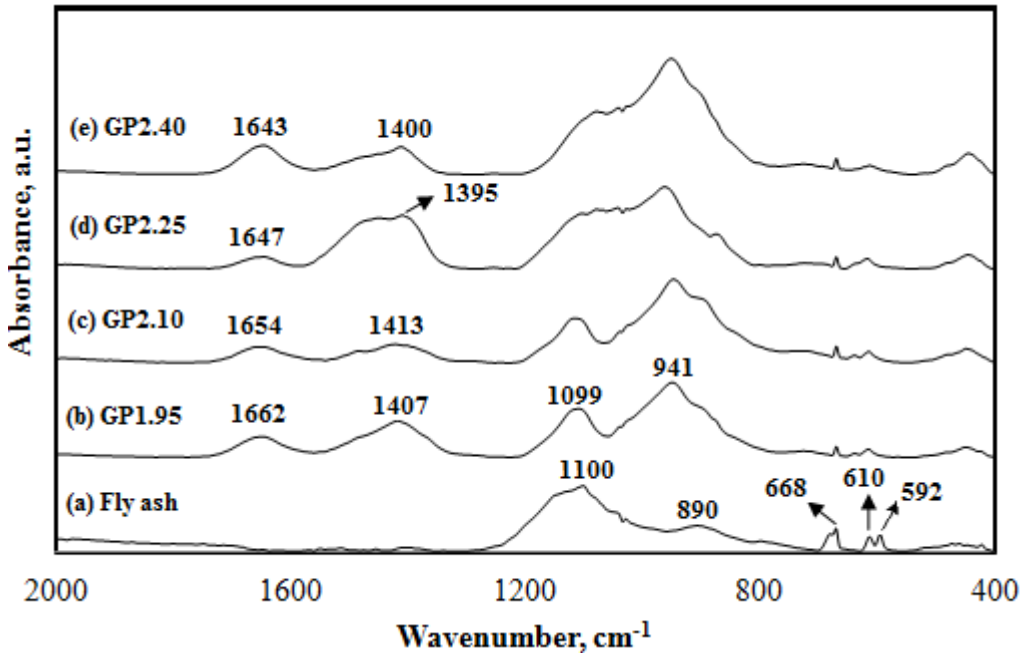

Figure 3.2. FTIR spectra of C type fly ash and fly ash based geopolymers **(a)** Fly ash, **(b)** GP1.95 (Si/Al ratio: 1.95), **(c)** GP2.10 (Si/Al ratio: 2.10), **(d)** GP2.25 (Si/Al ratio: 2.25), **(e)** GP2.40 (Si/Al ratio: 2.40).

As a result of alkali-activation of fly ash, the FTIR patterns are significantly transferred into a different form (Figure 3.2). First of all, the characteristic peaks indicating anhydrite disappeared in the FTIR spectra of geopolymer specimens. The FTIR spectrum of geopolmer with Si/Al ratio of 1.95 is dominated by two distinct broad features that are located at about 941 and 1099 cm^{-1}, respectively. With increasing Si/Al ratios, the intensity of the band at 945 cm^{-1} increases systematically and these two peaks merge. It is thought that these peaks could represent two phases, and these phases evolve with increasing Si content in the system. The distinct feature at 1099 cm^{-1} in this study can be related to asymmetric stretching mode of T-O-T bonds in sodium aluminosilicate hydrate (NASH) [96]. NASH gel is the main reaction product of alkali-activated aluminosilicates and therefore could have been formed in this system. On the other hand, the band positioned at 945 cm^{-1} is thought to be possibly related to calcium aluminosilicate hydrate (CASH) gel phase [96]. CASH phase can be present in Portland Cement pastes and may exhibit an FTIR band at 945 cm^{-1}. The FTIR spectra obtained in this part are quite consistent with the results of a recent study [96], where NASH and CASH gel phases were investigated by FTIR spectroscopy. It is thought that, in the presence of high CaO content, formation of CSH or CASH phases could also be possible. *Guo et al.* (2010) [97] also reported the

presence of a CSH gel phase together with a geopolymeric gel in type C fly ash-based geopolymers. In this context, the main band at 945 cm^{-1} could also be partly related to an amorphous aluminosilicate gel together with CSH or CASH structures. It should be noted that in a fly ash based geopolymer study, the main FTIR bands between 950-966 cm^{-1} were reported to be related to Si-O-T asymmetric stretching vibrations [98]. It should be also noted that, as obvious from the FTIR spectra this is a complicated system where multiple phases could be present in the structure. Furthermore, the bands positoned at around 1420 cm^{-1} reveals the calcium carbonate formation [38]. This fact is consistent with the samples as indicated from XRD patterns in Figure 3.1. The absorbtion bands located around 1660 cm^{-1} are related to OH bending means [83] that this region represents adsorbed water (Figure 3.2) [86].

Figure 3.3 shows scanning transmission microscopic images of C type fly ash and all fly ash based geopolymers. Spherical cenospheres can be observed in the microstructure of fly ash consistent with the literature [99]. However, these cenospheres vanished by alkali activation and gel formations are observed in geopolymer samples. CSH - like gel formation is observed in all samples supporting the hypothesis made above based on FTIR results.

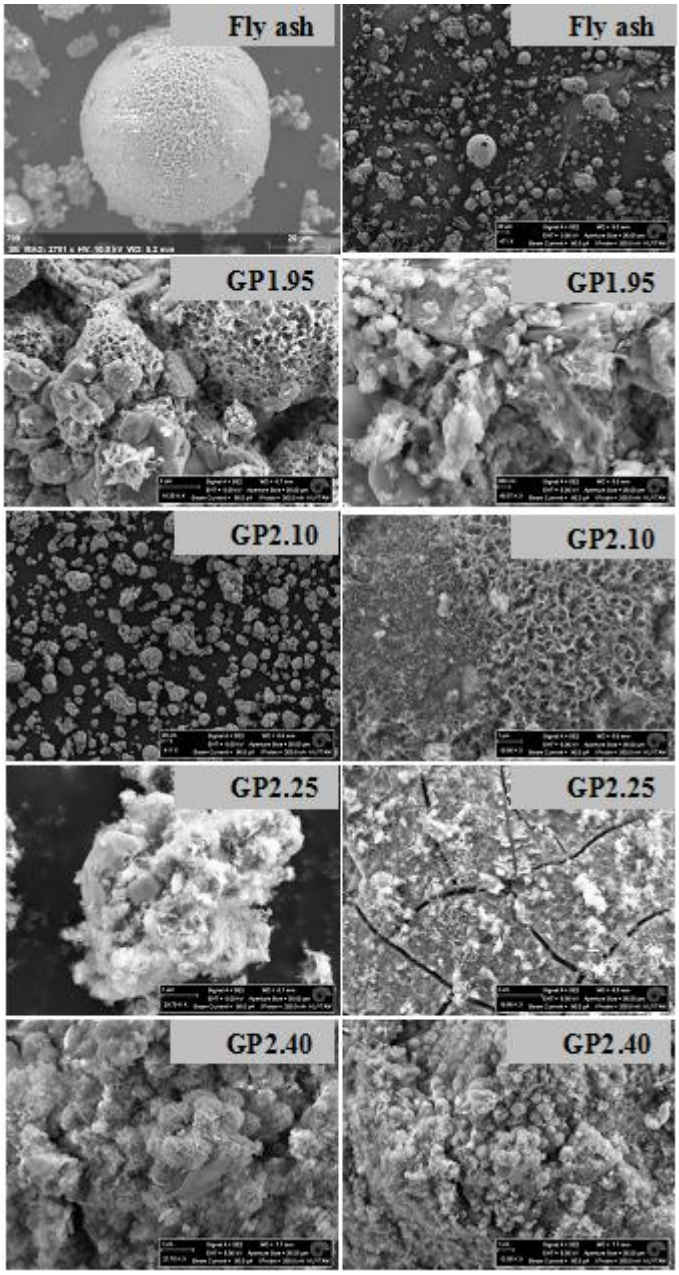

Figure 3.3. Scanning transmission microscopic images of C type fly ash and all fly ash based geopolymers.

Figure 3.4 displays the compressive strength values measured for the geopolymer samples produced as a function of molar Si/Al ratios in lignite fly ash based geopolymer structures. It is observed that geopolymer specimen with Si/Al molar ratio of 2.40 displays the highest compressive strength value of 7.15 MPa. As it is seen from all these results, increased Si content in the structure contributed to mechanical strength.

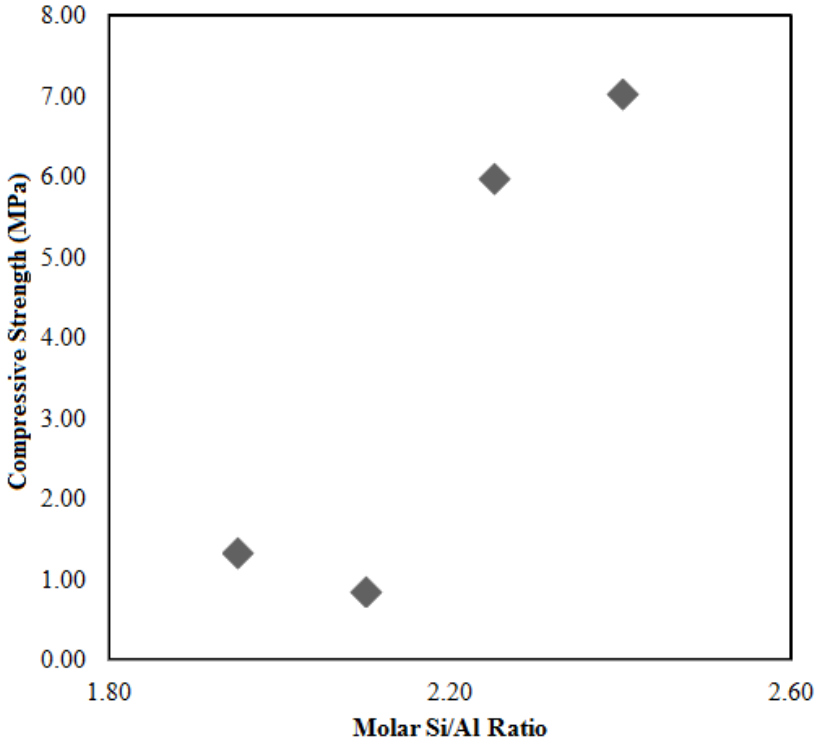

Figure 3.4. The compressive strength values measured for the geopolymer samples produced as a function of molar Si/Al ratios in C type fly ash based geopolymer structures.

3.3.2. Fly ash and Red Mud Based Geopolymers with Varying Red Mud Contents

Calcined red mud is obtained by thermal treatment at 800 ^{o}C for 3 hours. Figure 3.5 reveals the XRD patterns of calcined red mud, fly ash and fly ash-red mud based geopolymers investigated in this study.

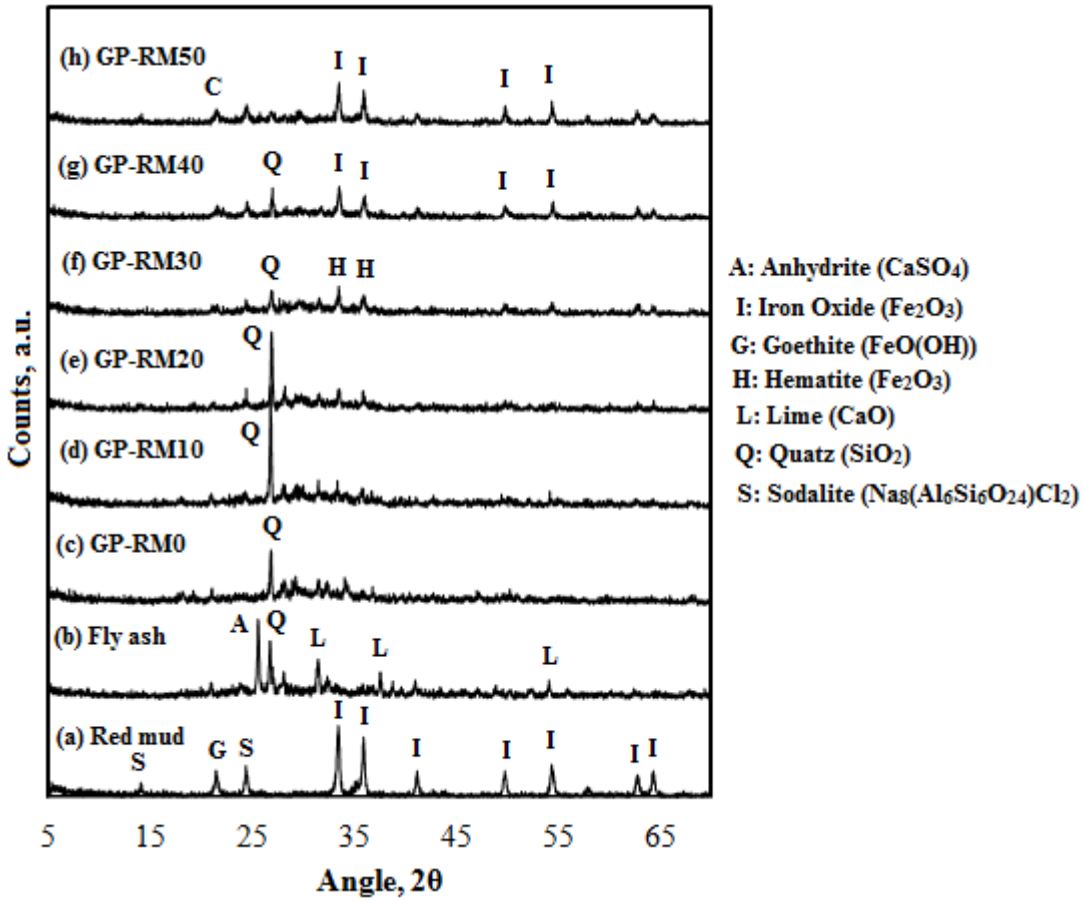

Figure 3.5. XRD patterns of red mud, fly ash and fly ash-red mud based geopolymers **(a)** Red mud, **(b)** Fly ash, **(c)** GP-RM0 (red mud content 0 %), **(d)** GP-RM10 (red mud content 10 %), **(e)** GP-RM20 (red mud content 20 %), **(f)** GP-RM30 (red mud content 30 %), **(g)** GP-RM40 (red mud content 40 %), **(h)** GP-RM50 (red mud content 50 %).

Anhydrite ($CaSO_4$), lime (CaO) and quartz (SiO_2) are the main crystalline compounds observed in the XRD pattern of fly ash (Figure 3.5). Calcined red mud consists of iron oxide (Fe_2O_3), goethite (FeO(OH)), sodalite ($Na_4Cl(Al_3Si_3O_{12})$) and quartz (SiO_2) phases (Figure 3.5). Fly ash-red mud raw material mixture prepared with different red mud contents (0-50 % red mud) were employed in geopolymerization in this part. As it is seen in Figure 3.5, the specimens containing 0 %, 10 % and 20 % red mud included mainly quartz crystalline phases. However, geopolymer samples with the composition of 30 %, 40 % and 50 % red mud display phases including hematite (Fe_2O_3) and iron oxide (Fe_2O_3) in a more distinct fashion. This can be due to remaining unreacted red mud present in these samples. As it is seen from these diffraction patterns, as red mud content increases,

geopolymerization process can be difficult owing to great amount of iron present in red mud.

FTIR spectra of lignite fly ash, calcined red mud and fly ash-red mud geopolymers with diffferent red mud compositions (0-50 %) are given in Figure 3.6. FTIR spectrum of fly ash displays low frequency bands seen at 592, 610 and 668 cm^{-1} that are related to anhydrite presence in the structure [90] as supported with the results of XRD (Figure 3.5). A broad band located around 890 cm^{-1} is assigned to C-O vibrations [90]. The main feature positioned at about 1100 cm^{-1} in the FTIR spectrum of fly ash is related to the asymmetric stretching vibrations of Si-O-Si and Al-O-Si in the structure [92-95]. Some small sharp peaks around 1490-1666 cm^{-1} observed in FTIR spectrum of fly ash is attributed to presence of Ca-O structure [100]. Low frequency band at 443 cm^{-1} in FTIR spectrum of red mud is related with Fe-O stretching vibrations [36,76]. Moreover, low frequency band at 603 cm^{-1} and high frequency band at 979 cm^{-1} in the FTIR spectrum of calcined red mud indicate Si-O stretching vibrations [100]. As a result of alkali-activation of fly ash-red mud system, the FTIR pattern of fly ash and red mud are completely transformed into a different form as it is seen in Fig 3.6. Similar to the previous part, this system displays the presence of two bands that merge as a function of increased red mud content. The band at 1114 cm^{-1} is assigned to asymmetric stretching mode of T-O-T bonds in NASH [96]. As mentioned in the previous part alkali activation of aluminosilicates could give rise to this phase. On the other hand, the band positioned at 941 cm^{-1} could be assigned to a CSH or CASH [91] gel based on the position of this band and considering the high amount of Ca in the system. With increased red mud content in the system it was observed that the peak located at 1114 cm^{-1} slightly moved to lower wavenumbers, and the peak at 941 cm^{-1} moved to higher frequencies. For the 40 or 50 % red mud containing geopolymer, the FTIR spectra are dominated by a strong feature at about 970 cm^{-1}. Considering the large width and the position of this band, the formation of an amorphous aluminosilicate phase is very likely for the high red mud containing geopolymers. This fact is consistent with the literature as geopolymers are known to give rise to a broad feature in 900-1200 cm^{-1} region. However, Ca is still present in the system (less compared to fly ash based geopolymer), the possibility of a minor amount of CASH or CSH phase could be still present.

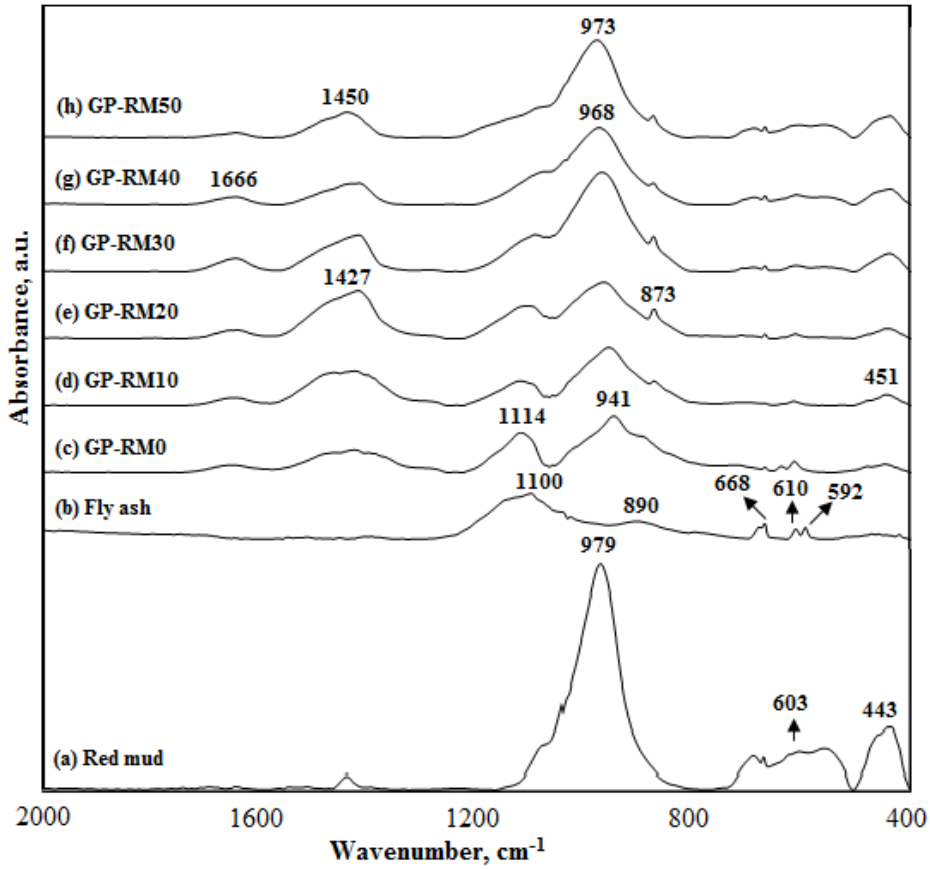

Figure 3.6. FTIR spectra of red mud, fly ash and fly ash-red mud based geopolymers **(a)** Red mud, **(b)** Fly ash, **(c)** GP-RM0 (red mud content 0 %), **(d)** GP-RM10 (red mud content 10 %), **(e)** GP-RM20 (red mud content 20 %), **(f)** GP-RM30 (red mud content 30 %), **(g)** GP-RM40 (red mud content 40 %), **(h)** GP-RM50 (red mud content 50 %).

The peaks around 451 cm^{-1} in all geopolymer specimes indicate the bending vibration of Si-O-Si bond (Figure 3.6) [99,91]. Sharp peaks around 873 cm^{-1} and 1427 cm^{-1} correspond to carbonate (CO_3) groups demonstrates a slight carboxilation of $Ca(OH)_2$ from carbondioxide of the atmosphere [101]. Stretching vibrations of C-O (carbonate) were observed in all obtained geopolymer samples at the peaks of between 1427 cm^{-1} and 1450 cm^{-1} [51,36,102,103]. The band located around 1666 cm^{-1} is associated with Ca-O structure [100].

Scanning electron micrographs of fly ash and red mud and fly ash-red mud based geopolymer samples are shown in Figure 3.7 and Figure 3.8, respectively. As it is shown in Figure 3.7, spherical cenospheres can be observed in the microstructure of fly ash [99]. Red mud displayed flaky shaped particles consistent with literature (Figure 3.7) [12].

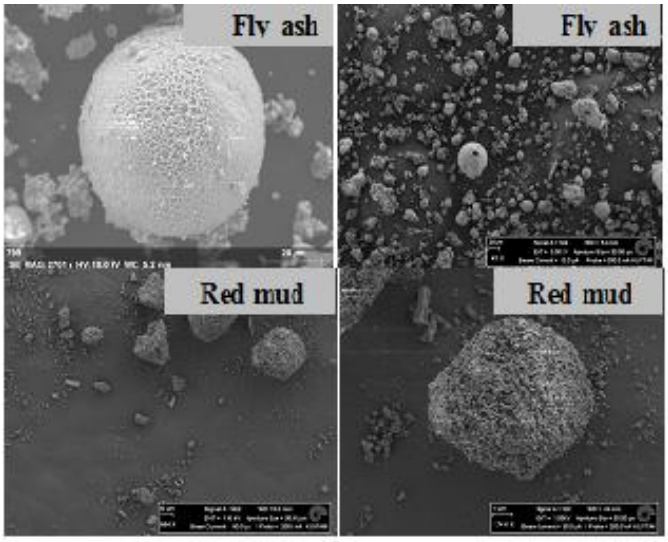

Figure 3.7. Scanning electron micrographs of fly ash and red mud.

As a result of alkali activation, cenospheres seen in fly ash vanished and gel formations are observed in geopolymer samples (Figure 3.8). Based on FTIR results it is thought that CSH and CASH gel phases could have formed. SEM images display gel-like features for specimens with red mud content 0 % - 30 %. Small microspheres are observed in the sample produced with 30 % red mud. These microspheres show the structure of hematite [36]. For geopolymers with red mud content 40 and 50 %, SEM miscrostructures display glassy morphologies consistent with the broad FTIR main bands for these samples.

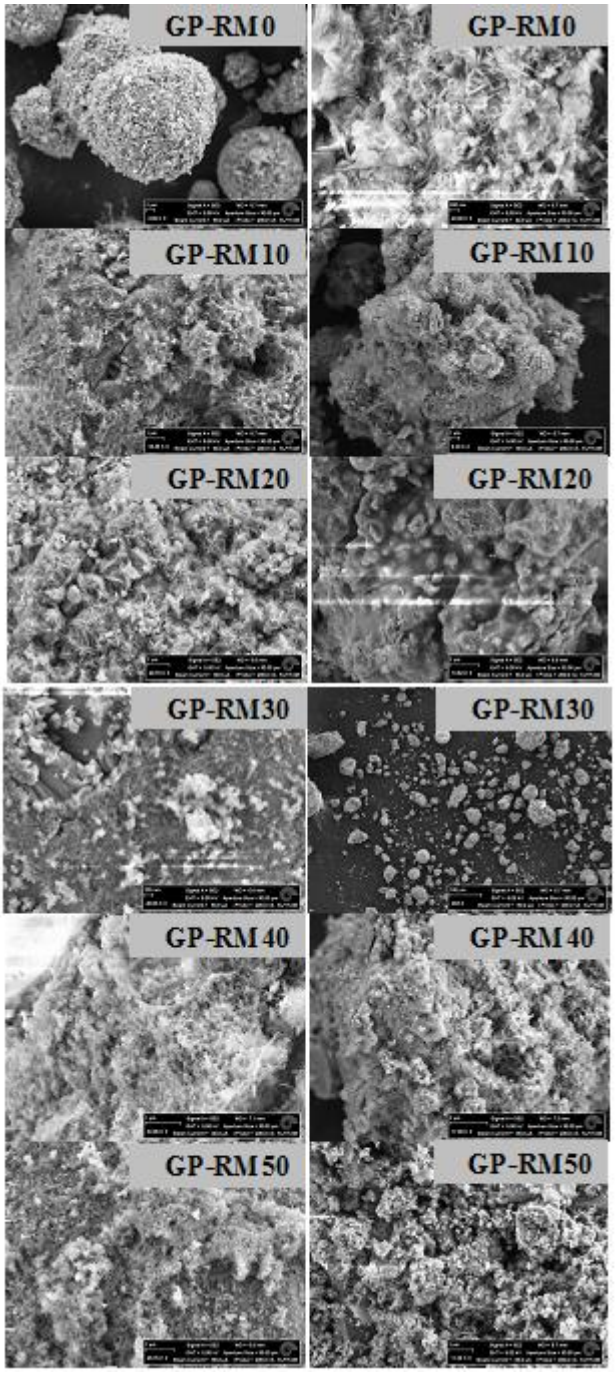

Figure 3.8. Scanning electron micrographs of fly ash-red mud based geopolymer samples.

Compressive strength values for fly ash-red mud based samples as a function of red mud composition are given in Figure 3.9. Although these values seem to be rather low for engineering applications, it should be mentioned that the composition of 20 % red mud has highest compressive strength value of 6.56 MPa. The possible reasons for these low compressive strength values possibly arise from use of untreated fly ash in the

geopolymerization or the high Fe_2O_3 content in red mud that possibly does not take part in geopolymerization.

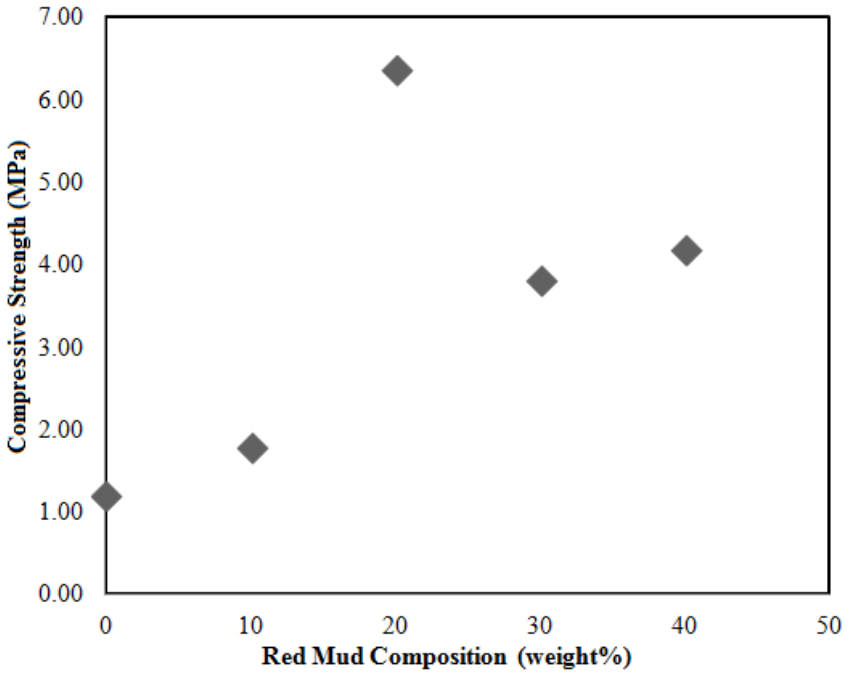

Figure 3.9. Compressive strength values for fly ash-red mud based samples as a function of red mud composition.

3.4. Conclusions

C type fly ash based geopolymers with molar Si/Al ratios between 1.95 and 2.40 and fly ash-red mud based geopolymers with varying red mud contents (0-50 %) were synthesized and characterized by XRD, FTIR spectroscopy, and SEM. Compressive strength analysis were performed on produced samples. In C type fly ash based geopolymers the possible presence of two phases have been identified by FTIR spectroscopy. It was seen that FTIR spectrum of C type fly ash based geopolymer with molar Si/Al ratio of 1.95 displays two bands located at 941 cm^{-1} and 1141 cm^{-1}, possibly corresponding to i) amorphous aluminosilicate gel together with calcium aluminosilicate hydrate (CASH) and/or calcium silicate hydrate (CSH) and ii) sodium aluminosilicate hydrate (NASH) gel, respectively. These two features were observed to merge together as a function of increasing molar Si/Al ratio in the system with an accompanied increase in the corresponding compressive strength values. On the other hand, structural features of fly

ash-red mud based geopolymers with low red mud contents are found similar to fly ash based geopolymers. Geopolymer samples with red mud content between 0 % - 30 % seemed to mainly include calcium aluminosilicate silicate hydrate (CASH) and/or calcium silicate hydrate (CSH) gels together with sodium aluminosilicate hydrate (NASH) gel. The FTIR bands corresponding to these phases merge together with increasing red mud content in the system indicating possible interaction between phases. This possible transition from a two-phase system into a relatively uniform phase in geopolymer system is thought to be responsible for the increasing trends in compressive strength values.

4. CONCLUSIONS AND RECOMMENDATIONS

4.1. Conclusions

The aim of this thesis is to understand correlations between structure and performance of metakaolin, fly ash and red mud based geopolymers. Metakaolin based samples with molar Si/Al ratios of 1.12, 1.77 and 2.20; class C fly ash based geopolymers with different Si/Al molar ratios of 1.95, 2.10, 2.25, 2.40; and class C fly ash and red mud based geopolymers with different red mud composition in the region of 0-50 % were synthesized and characterized by XRD, FTIR spectroscopy, and SEM. Compressive strength measurements were also performed on the all produced specimens.

It was found in first study that samples with Si/Al ratio of 1.12 consist of crystalline components including zeolite A and/or sodalite. These samples were not mechanically strong owing to their highly crystalline structure with compressive strength values of around 1 MPa. XRD patterns show that geopolymers with molar Si/Al ratios of 1.77 and 2.20 have amorphous structure and glassy SEM images indicate that these samples have glassy microstructures. FTIR spectra of these geopolymers reveal that main band in the region of 900-1200 cm^{-1} represents geopolymerization and as molar Si/Al ratio increases, it moved orderly to higher frequencies. This behaviour of this band was shown to be proportional to increases in the compressive strength values.

On the other hand, in second study, amorphous aluminosilicate gel together with calcium aluminosilicate hydrate (CASH) or calcium silicate hydrate (CSH) and sodium aluminosilicate hydrate (NASH) formations can be observed in C type fly ash based geopolymer structure. In addition, similar structures can be detected in produced geopolymer specimens with red mud content 0 % - 30 % whereas geopolymer samples with red mud content 40 and 50 % display relatively uniform amorphous aluminosilicate structure. Moreover, it was observed that geopolymer sample containing 20 % red mud has highest compressive strength value of 6.56 MPa. It was detected that obtained geopolymer

sample with Si/Al molar ratio of 2.40 has highest compressive strength value of 7.15 MPa. This result points out that Si contributes to forming a more stable structure.

4.2. Recommendations

Some aggregates such as sand can be mixed with raw materials used here (metakaolin, fly ash and red mud) to increase compressive strength of samples.

Geopolymer synthesis can be performed by changing heat treatment of raw meaterials and curing conditions. Fly ash used in geopolymer synthesis as a raw material could be treated at different temperatures.

Different molarity of alkali activator can be used to produce metakaolin based geopolymer samples.

Moreover, structural findings can be correlated to new physical properties such as pore size distribution and modeling methods can be used to complement the findings of this experimental work.

Thermal conductivities of geopolymer samples may be measured due to detect whether they are convenient or not to be used as construction materials.

REFERENCES

1. Vijaya Rangan, B., ‘‘Fly Ash-Based Geopolymer Concrete’’, *Proceedings of the International Workshop on Geopolymer Cement and Concrete*, Allied Publishers Private Limited, Mumbai, India, pp. 68-106, 2010.

2. McCaffrey, R., ‘‘Climate change and the cement industry’’, *Global Cement and Lime Magazine (Environmental Special Issue)*, pp. 15-19, 2002.

3. Shi, C., A. Fernández Jiménez, A. Palomo, “New Cements for the 21st Century: The pursuit of an Alternative to Portland Cement’’, *Cement and Concrete Research*, Vol. 41, No. 7, pp. 750-763, 2011.

4. Turner, L. K., F.G. Collins, “Carbon Dioxide Equivalent (CO_2-e) Emissions: A Comparison Between Geopolymer and OPC Cement Concrete’’, *Construction and Building Materials*, Vol. 43, No. 6, pp. 125-130, 2013.

5. Huntzinger, D. N., T. D. Eatmon, “A life-cycle Assessment of Cement Manufacturing: Comparing Traditional Process with Alternative Technologies’’, *Journal of Cleaner Production*, Vol. 17, No. 7, pp. 668-675, 2009.

6. Meyer, C., “The Greening of the Concrete Industry’’, *Cement and Concrete Composites*, Vol. 31, No. 8, pp. 601-605, 2009.

7. Joseph, B., G. Mathew, “Influence of Aggregate Content on the Behavior of Fly Ash Based Geopolymer Concrete’’, *Scientia Iranica*, Vol. 19, No. 5, pp. 1188-1194, 2012.

8. Malhotra, V. M., ‘‘Introduction: Sustainable Development and Concrete Technology’’, *American Concrete Institute*, Vol. 24, No. 7, p. 22, 2002.

9. White, C. E, J. L. Provis, T. Proffen, Daniel P. Riley, J. S. J. Van Deventer, ‘‘Solving the Structure of Metakaolin’’, *Nature Materials*, 2009.

10. Duxson, P., J. L. Provis, G. C. Lukey, J. S. J. Van Deventer, ‘‘The Role of Inorganic Polymer Technology in the Development of 'Green Concrete'’’, *Cement and Concrete Research*, Vol. 37, No. 12, pp. 1590-1597, 2007.

11. Provis, J. L., J. S. J. Van Deventer, *Geopolymers: Structures, Processing, Properties and Industrial Applications*, Woodhead, Cambridge, UK, 2009.

12. Zhang, M., T. El-Korchi, G. Zhang, J. Liang, M. Tao, ‘‘Synthesis Factors Affecting Mechanical Properties, Microstructure, and Chemical Composition of Red Mud-Fly ash Based Geopolymers’’, *Fuel*, Vol. 134, pp. 315-325, 2014.

13. Davidovits, J., ‘‘Properties of Geopolymer Cements’’, *First international conference on alkaline cements and concretes*, Kiev, Ukraine, 1994.

14. Zhang., G., J. He, R. P. Gambrell, ‘‘Synthesis, Characterization, and Mechanical Properties of Red Mud-Based Geopolymers’’, *Transportation Research Record*, Vol. 2167, pp. 1-9, 2010.

15. Gao, K., K. L. Lin, D. Y. Wanga, C. L. Hwang, B. L. Anh Tuan, H. S. Shiu, T. W. Cheng, ‘‘Effect of Nano-SiO_2 on the Alkali-Activated Characteristics of Metakaolin-Based Geopolymers’’, *Construction and Building Materials*, Vol. 48, pp. 441-447, 2013.

16. Davidovits, J., ‘‘Geopolymers and Geopolymer New Materials’’, *Journal of Thermal Analysis*, Vol. 35, No. 2, pp. 429-441, 1989.

17. Van Jaarsveld, J. G. S., J. S. J. Van Deventer, L. Lorenzen, ‘‘The Potential Use of Geopolymer Materials to Immobilize Toxic Metals: Part I: Theory and Applications’’, *Minerals Engineering*, Vol. 10, No. 7, pp. 659-669, 1997.

18. Zhang, Y. S., W. Sun, Z. J. Li, ‘‘Composition Design and Microstructural Characterization of Calcined Kaolin-Based Geopolymer Cement’’, *Applied Clay Science*, Vol. 47, No. 3-4, pp. 271-275, 2010.

19. Davidovits, J., ‘‘The Poly(Sialate) Terminology: A Very Useful and Simple Model for the Promotion and Understanding of Green Chemistry’’, *Geopolymer Chemistry and Sustainable Development Solutions*, 2005.

20. Van Jaarsveld, J. G. S., J. S. J. Van Deventer, G. C. Lukey, ‘‘The Effect of Composition and Temperature on the Properties of Fly Ash- and Kaolinite-Based Geopolymers’’, *Chemical Engineering Journal*, Vol. 89, No. 1-3, pp. 63-73, 2002.

21. Lin, K. L., H. S. Shiu, J. L. Shie, T. W. Cheng, C. L. Hwang, ‘‘Effect of Composition on Characteristics of Thin Film Transistor Liquid Crystal Display (TFT-LCD) Waste Glass-Metakaolin-Based Geopolymers’’, *Construction and Building Materials*, Vol. 36, pp. 501-507, 2012.

22. USGS: Mineral Commodity Summary, ‘‘Major Producers of Kaolin in World-2010’’, 2011, http://www.mapsofworld.com/minerals/world-kaolin-producers.html, [Accessed June 2015].

23. Kamseu, E., A. Rizzuti, C. Leonelli, D. Perera, ‘‘Enhanced Thermal Stability in K_2O Metakaolin-Based Geopolymer Concretes by Al_2O_3 and SiO_2 Fillers Addition’’, *Journal of Material Science*, Vol. 45, No. 7, pp. 1715-1724, 2010.

24. Sperinck, S. and Raiteri, P., N. Marks, K. Wright, ‘‘Dehydroxylation of Kaolinite to Metakaolin - A Molecular Dynamics Study’’, *Journal of Materials Chemistry*, Vol. 21, No. 7, p. 2123, 2011.

25. Gordon, L. E., R. S. Nicolas, J. L. Provis, ‘‘Chemical Characterisation of Metakaolin and Fly Ash Based Geopolymers During Exposure to Solvents Used in Carbon Capture’’, *International Journal of Greenhouse Gas Control*, Vol. 27, pp. 255-266, 2014.

26. Görhan, G., G. Kürklü, ‘‘The Influence of the NaOH Solution on the Properties of the Fly Ash-Based Geopolymer Mortar Cured at Different Temperatures’’, *Composites: Part B*, Vol. 58, pp. 371-377, 2014.

27. Yıldırım, H., M. Sümer, V. Akyüncü, E. Gürbüz, ‘‘Comparison on Efficiency Factors of F and C Types of Fly Ashes’’, *Construction and Building Materials*, Vol. 25, No. 6, pp. 2939-2947, 2011.

28. Helmuth, R. , *Fly Ash in Cement and Concrete*, Portland Cement Association, Skokie, IL, 1987.

29. Kabay, N., M. Mansur Tufekci, A. B. Kızılkanat, D. Oktay, ‘‘Properties of Concrete with Pumice Powder and Fly Ash as Cement Replacement Materials’’, *Construction and Building Materials*, Vol. 85, pp. 1-8, 2015.

30. ‘‘ASTM C618 Standard Specification for Coal Fly Ash and Raw or Calcined Natural Pozzolan for Used in Concrete’’, 2012.

31. Yılmaz, H., ‘‘Characterization and Comparison of Leaching Behaviors of Fly Ash Samples from Three Different Power Plants in Turkey’’, *Fuel Processing Technology*, Vol. 137, pp. 240-249, 2015.

32. Öner, A., S. Akyüz, R. Yıldız, ‘‘An Experimental Study on Strength Development of Concrete Containing Fly Ash and Optimum Usage of Fly Ash in Concrete’’, *Cement and Concrete Research*, Vol. 35, No. 6, pp. 1165-1171, 2005.

33. He, J., Y. Jie, J. Zhang, Y. Yu, G. Zhang, “Synthesis and Characterization of Red Mud and Rice Husk Ash-Based Geopolymer Composites”, *Cement and Concrete Composites*, Vol. 37, pp. 108-118, 2013.

34. Hanjitsuwan, S., S. Hunpratub, P. Thongbai, S. Maensiri, V. Sata, P. Chindaprasirt, “Effects of NaOH Concentrations on Physical and Electrical Properties of High Calcium Fly Ash Geopolymer Paste”, *Cement and Concrete Composites*, Vol. 45, pp. 9-14, 2014.

35. Heysung Kım, E., *Understanding Effects of Silicon/Aluminum Ratio and Calcium Hydroxide on Chemical Composition, Nanostructure and Compressive Strength for*

Metakaolin Geopolymers, M.S. Thesis, Graduate College of the University of Illinois at Urbana-Champaign, 2012.

36. Kumar, A., S. Kumar, "Development of Paving Blocks from Synergistic Use of Red Mud and Fly Ash Using Geopolymerization", *Construction and Building Materials*, Vol. 38, pp. 865-871, 2013.

37. Meral, C., C. J. Benmore, P. J. M. Monteiro, "The Study of Disorder and Nanocrystallinity in C-S-H, Supplementary Cementitious Materials and Geopolymers Using Pair Distribution Function Analysis" , *Cement and Concrete Research*, Vol. 41, No. 7, pp. 696-710, 2011.

38. Temuujin, J., A. Minjigmaa, B. Davaabal, U. Bayarzul, A. Ankhtuya, Ts. Jadambaa, K. J. D. MacKenzie, "Utilization of Radioactive High-Calcium Mongolian Fly Ash for the Preparation of Alkali-Activated Geopolymers for Safe Use as Construction Materials", *Ceramics International*, Vol. 40, No. 10, pp. 16475-16483, 2014.

39. Duxson, P., A. Fernández-Jiménez, J. L. Provis, G. C. Lukey, A. Palomo, J. S. J. Van Deventer, "Geopolymer Technology: the Current State of the Art'', *Journal of Materials Science*, Vol. 42, No. 9, pp. 2917-2933, 2006.

40. Davidovits, J., *Proceedings of Geopolymer '88-First European Conference on Soft Mineralurgy*, eds. J. Davidovits, J. Orlinski, Universite De Technologie De Compeigne, Compeigne, France, pp. 149-166, 1988.

41. Rovnaník, P., "Effect of Curing Temperature on the Development of Hard Structure of Metakaolin-Based Geopolymer'', *Construction and Building Materials*, Vol. 24, No. 7, pp. 1176-1183, 2010.

42. Liew, Y. M., H. Kamarudin, A. M. Mustafa Al Bakri, M. Bnhussain, M. Luqman, I. Khairul Nizar, C. M. Ruzaidi, C. Y. Heah, "Optimization of Solids-to-Liquid and Alkali Activator Ratios of Calcined Kaolin Geopolymeric Powder'', *Construction and Building Materials*, Vol. 37, pp. 440-451, 2012.

43. Stubican, V., R. Roy, "Isomorphous Substitution and Infrared Spectra of Lattice Layer Silicates'', *American Mineralogist*, Vol. 46, pp. 32-51, 1961.

44. Flanigan, E. M., H. Khatami, H. A. Szymanski, "Molecular Sieve Zeolites'', *Advances in Chemistry Series*, Vol. 101, American Chemical Society, Washington, DC, pp. 201-229, 1971.

45. Arioz, E., O.Arioz, O. M. Kockar, "Leaching of F-type Fly Ash Based Geopolymers'', 20th International Congress of Chemical and Process Engineering CHISA, *Procedia Engineering*, Vol. 42, pp. 1115-1117, 2012.

46. Mustafa Al Bakri, A. M., H. Kamarudin, M. BinHussain, I. Khairul Nizar, Y. Zarina, A.R. Rafiza, "The Effect of Curing Temperature on Physical and Chemical Properties of Geopolymers'', *Physics Procedia*, Vol. 22, pp. 289-290, 2011.

47. Varela, B., N. Privorotskaya, "The Use of Geopolymers as Concrete Coatings for Fire Protection'', *Geopolymer, Green Chemistry and Sustainable Development Solutions*, ed. J. Davidovits, France, 2005.

48. Muñiz-Villarreal, M. S., A. Manzano-Ramírez, S. Sampieri-Bulbarela, J. Ramón Gasca-Tirado, J. L. Reyes-Araiza, J. C. Rubio-Ávalos , J. J. Pérez-Bueno , L. M. Apatiga , A. Zaldivar-Cadena , V. Amigó-Borrás, "The Effect of Temperature on the Geopolymerization Process of a Metakaolin-Based Geopolymer'', *Materials Letters*, Vol. 65, No. 6, pp. 995-998, 2011.

49. Ferone, C., F. Colangelo, G. Roviello, D. Asprone, C. Menna , A. Balsamo, A. Prota, R. Cioffi and G. Manfredi, "Application-Oriented Chemical Optimization of a Metakaolin Based Geopolymer'', *Materials*, 2013.

50. P. Duxson, J. L. Provis, G. C. Lukey, , S. W. Mallicoat., W. M. Kriven, J. S. J. Van Deventer, "Understanding the Relationship Between Geopolymer Composition, Microstructure and Mechanical Properties'', *Colloids and Surfaces A: Physicochemical and Engineering Aspects*, Vol. 269, No. 1-3, pp. 47-58, 2005.

51. Ye, N., J. Yang, X. Ke, J. Zhu, Y. Li, C. Xiang, H. Wang, L. Li, and B. Xiao, "Synthesis and Characterization of Geopolymer from Bayer Red Mud with Thermal Pretreatment'', *Journal of American Ceramic Society*, Vol. 97, No. 5, pp. 1652-1660, 2014.

52. Xie, T., T. Ozbakkaloglu, ''Behavior of Low-Calcium Fly and Bottom Ash-Based Geopolymer Concrete Cured at Ambient Temperature'', *Ceramics International*, Vol. 41, No. 4, pp. 5945-5958, 2015.

53. Rahier, H., B. Van Mele, M. Biesemans, J. Wastiels, X. Wu, ''Low-Temperature Synthesized Aluminosilicate Glasses .1. Low-temperature Reaction Stoichiometry and Structure of a Model Compound'', *Journal of Materials Science*, Vol. 31, No. 1, pp. 71-79, 1996.

54. Krivenko, P. V., *Proceedings of the First International Conference on Alkaline Cements and Concretes*, ed. P. V. Krivenko, VIPOL Stock Company, Kiev, Ukraine, Vol. 1, pp. 11-129, 1994.

55. Mallicoat, S., P. Sarin, W.M. Kriven, ''Novel Alkali-Bonded Ceramic Filtration Membranes'', eds. M. E. Brito, P. Filip, C. Lewinsohn, A. Sayir, M. Opeka, W. M. Mullins, D. Zhu and W. M. Kriven, *Ceramic Engineering and Science Proceedings*, Vol. 26, No. 8, pp. 37-44, 2005.

56. Bao, Y., M. W. Grutzeck, C. M. Jantzen, ''Preparation and Properties of Hydroceramic Waste Forms Made with Simulated Hanford Low-Activity Waste'', *Journal of the American Ceramic Society*, Vol. 88, No. 12, pp. 3287-3302, 2005.

57. Davidovits, J., ''Geopolymers: Inorganic Polymeric New Materials'', *Journal of Thermal Analysis*, Vol. 37, No. 8, pp. 1633-1656, 1991.

58. Rowles, M., B. O'Connor, ''Chemical Optimisation of the Compressive Strength of Aluminosilicate Geopolymers Synthesised by Sodium Silicate Activation of Metakaolinite'', *Journal of Materials Chemistry*, Vol. 13, pp. 1161-1165, 2003.

59. Mohd Salahuddin, M. B., M. Norkhairunnisa, F. Mustapha, ‘‘A Review on Thermophysical Evaluation of Alkali-Activated Geopolymers’’, *Ceramics International*, Vol. 41, No. 3, pp. 4273-4281, 2015.

60. Dimas, D. D., I. P. Giannopoulou, D. Panias, ‘‘Utilization of Alumina Red Mud for Synthesis of Inorganic Polymeric Materials’’, *Mineral processing and extractive metallurgy review: An International Journal*, Vol. 30, No. 3, pp. 211-239, 2009.

61. Hajjaji, W., S. Andrejkovicova, C. Zanelli, M. Alshaaer, M. Dondi, J. A. Labricha, F. Rocha, ‘‘Composition and Technological Properties of Geopolymers Based on Metakaolin and Red Mud’’, *Materials&Design*, Vol. 52, pp. 648-654, 2013.

62. He, J., G. Zhang, ‘‘Geopolymerization of Red Mud and Fly Ash for Civil Infrastructure Applications’’, *Geo-Frontiers*, pp. 1287-1296, 2011.

63. Williams, R. P., A. van Riessen, ‘‘Development of Alkali Activated Borosilicate Inorganic Polymers’’, *Journal of the European Ceramic Society*, Vol. 31, No. 8, pp. 1513-1516, 2011.

64. Duxson, P., S. W. Mallicoat, G. C. Lukey, W. M. Kriven, J. S. J. Van Deventer, ‘‘The Effect of Alkali and Si/Al Ratio on the Development of Mechanical Properties of Metakaolin Based Geopolymers’’, *Colloids Surface A*, Vol. 292, No. 1, pp. 8-20, 2007.

65. Steveson, M., K. Sagoe-Crentsil, ‘‘Relationships Between Composition, Structure and Strength of Inorganic Polymers Part 2 Fly Ash-Derived Inorganic Polymers’’, *Journal of Materials Science*, Vol. 40, No. 16, pp. 4247-4259, 2005.

66. White, C. E. , J. L. Provis, T. Proffen, D. P. Riley, J. S. J. Van Deventer, ‘‘Density Functional Modeling of the Local Structure of Kaolinite Subjected to Thermal Dehydroxylation’’, *Journal of Physical Chemistry A*, Vol. 114, No. 14, pp. 4988-4996, 2010.

67. Reyes, C. A. R., C. Williams, O. M. C. Alarcón, ‘‘Nucleation and Growth Process of Sodalite and Cancrinite from Kaolinite-Rich Clay under Low-Temperature Hydrothermal Conditions’’, *Materials Research*, Vol. 16, No. 2, pp. 424-438, 2013.

68. Hoch, M. and A. Bandara, ‘‘Determination of the Adsorption Process of Tributyltin (TBT) and Monobutyltin (MBT) onto Kaolinite Surface Using Fourier Transform Infrared (FT-IR) Spectroscopy’’, *Colloids Surface A*, Vol. 253, No. 1-3, pp. 117-124, 2005.

69. Zhao, H., Y. Deng, J. B. Harsh, M. Flury and J. S. Boyle, ‘‘Alteration of Kaolinite to Cancrinite and Sodalite by Simulated Hanford Tank Waste and Its Impact on Cesium Retention’’, *Clays and Clay Minerals*, Vol. 52, No. 1, pp. 1-13, 2004.

70. Lambert, J. F., W. S. Minman, J. J. Fripiat, ‘‘Revisiting Kaolinite Dehydroxylation: A Silicon-29 and Aluminum-27 MAS NMR Study’’, *Journal of the American Chemical Society*, Vol. 111, No. 10, pp. 3517-3522, 1989.

71. Saikia, B. J., G. Parthasarathy, ‘‘Fourier Transform Infrared Spectroscopic Characterization of Kaolinite from Assam and Meghalaya, Northeastern India’’, *International Journal of Modern Physics A*, Vol. 1, pp. 206-210, 2010.

72. Kim, D., Choi and S. Kim, ‘‘Sonochemical Synthesis of Zeolite A from Metakaolinite in NaOH Solution’’, *Materials Transactions*, Vol. 51, No. 9, pp. 1694-1698, 2010.

73. Markovic, S., V. Dondur, R. Dimitrijevic, ‘‘FTIR Spectroscopy of Framework Aluminosilicate Structures: Carnegieite and Pure Sodium Nepheline’’, *Journal of Molecular Structure*, Vol. 654, No. 1-3, pp. 223-234, 2003.

74. Heller-Kallai, L., I. Lapides, ‘‘Reactions of Kaolinites and Metakaolinites with NaOH-Comparison of Different Samples’’, *Applied Clay Science*, Vol. 35, No. 1-2, pp. 99-107, 2007.

75. Zaharaki, D., K. Komnitsas, V. Perdikatsiz, ‘‘Use of Analytical Techniques for identification of Inorganic Polymer Gel Composition’’, *Journal of Materials Science*, Vol. 45, pp. 2715-2724, 2010.

76. Gadsden, J. A., *Infrared Spectra of Minerals and Related Inorganic Compounds*, *Butterworths*, London, 1975.

77. Fernandez-Jimenez, A. and A. Palomo, ‘‘Composition and Microstructure of Alkali Activated Fly Ash Mortars: Effect of the Activator’’, *Cement and Concrete Research*, Vol. 35, pp. 1984-1992, 2005.

78. Chindaprasirt, P., T. Chareerat, V. Sirivivatnanon, ‘‘Workability and Strength of Coarse High Calcium Fly Ash Geopolymer’’, *Cement & Concrete Composites*, Vol. 29, No. 3, pp. 224-229, 2007.

79. Maholtra, V. M., ‘‘Introduction: Sustainable Development and Concrete Technology’’, *ACI Concrete International*, Vol. 24, No. 7, p. 22, 2002.

80. Tho-in, T., V. Sata, P. Chindaprasirt, C. Jaturapitakkul, ‘‘Pervious High-Calcium Fly Ash Geopolymer Concrete’’, *Construction and Building Materials*, Vol. 30, No. 325, pp. 366-371, 2012.

81. Temuujin, J., R. P. Williams, A. van Riessen, ‘‘Effect of Mechanical Activation of Fly Ash on the Properties of Geopolymer Cured at Ambient Temperature’’, *Journal of Materials Processing Technology*, Vol. 209, No. 12-13, pp. 5276-5280, 2009.

82. Komnitsas, K., and D. Zaharaki, ‘‘Geopolymerization: a Review and Prospects for the Minerals Industry’’, *Minerals Engineering*, Vol. 20, No. 14, pp. 1261-1277, 2007.

83. Rattanasak, U., P. Chindaprasirt, ‘‘Influence of NaOH Solution on the Synthesis of Fly Ash Geopolymer’’, *Minerals Engineering*, Vol. 22, No. 12, pp. 1073-1078, 2009.

84. Van Jaarsveld, J. G. S., J. S. J. Van Deventer, ‘‘Effect of the Alkali Metal Activator on the Properties of Fly Ash-Based Geopolymer’’, *Industrial and Engineering Chemistry Research*, Vol. 88, pp. 3932-3941, 1999.

85. Xu, H., J. S. J., Van Deventer, ‘‘The Geopolymerisation of Natural Alumino-Silicates’’, *Proceedings of the 2nd International Conference on Geopolymer*, pp. 43-63, France, 1999.

86. Swanepoel, J. C., C. A. Strydom, ‘‘Utilisation of Fly Ash in a Geopolymeric Material’’, *Applied Geochemistry*, Vol. 17, No. 8, pp. 1143-1148, 2002.

87. ‘‘ASTMC618 Standard Specification for Coal Fly Ash and Raw or Calcined Natural Pozzolan for Use in Concrete’’, *ASTM International*, 2013.

88. Cooling, D. J., D. J. Glenister, ‘‘Practical Aspects of Dry Residue Disposal’’, *Journal of Light Metals*, pp. 25-31, 1992.

89. Piga, F. P., L. Stoppa, ‘‘Recovering Metals from Red Mud Generated During Alumina Production’’, *JOM*, Vol. 45, No. 11, pp. 54-59, 1993.

90. Putnis, A., B. Winkler, L. Fernandez-Diaz, ‘‘In situ IR Spectroscopic and Thermogravimetric Study of the Dehydration of Gypsum’’, *Mineralogical Magazine*, Vol. 54, No. 374, pp. 123-128, 1990.

91. García Lodeiro, I., D. E. Macphee, A. Palomo, A. Fernández-Jiménez, ‘‘Effect of Alkalis on Fresh C-S-H Gels. FTIR Analysis’’, *Cement and Concrete Research*, Vol. 39, No. 3, pp. 147-153, 2009.

92. Perná, I., T. Hanzlíček, M. Šupová, ‘‘The Identification of Geopolymer Affinity in Specific Cases of Clay Materials’’, *Applied Clay Science*, Vol. 102, pp. 213-219, 2014.

93. Madejová, J., ‘‘FTIR Techniques in Clay Mineral Studies’’, *Vibrational Spectroscopy*, Vol. 31, No. 1, pp. 1-10, 2003.

94. Oréfice, R. L., W. L. Vasconcelos, ‘‘Sol-Gel Transition and Structural Evolution on Multicomponent Gels Derived from the Alumina-Silica System’’, *Journal of Sol-Gel Science and Technology*, Vol. 9, No. 3, pp. 239-249, 1997.

95. Lee, W. K. W., J. S. J. Van Deventer, ‘‘Use of Infrared Spectroscopy to Study Geopolymerization of Heterogeneous Amorphous Aluminosilicates’’, *Langmuir*, Vol. 19, No. 21, pp. 8726-8736, 2003.

96. Garcia-Lodeiro, I., I., A. Palomo, A. Fernández-Jiménez, D. E. Macphee, ‘‘Compatibility Studies Between N-A-S-H and C-A-S-H Gels. Study in the Ternary Diagram Na_2O-CaO-Al_2O_3-SiO_2-H_2O’’, *Cement and Concrete Research*, Vol. 41, No. 9, pp. 923-931, 2011.

97. Guo, X., H. Shi, W. A. Dick, ‘‘Compressive Strength and Microstructural Characteristics of Class C Fly Ash Geopolymer’’, *Cement and Concrete Composites*, Vol. 32, No. 2, pp. 142-147, 2010.

98. Marjanović, N., M. Komljenović , Z. Baščarević , V. Nikolić, ‘‘Improving Reactivity of Fly Ash and Properties of Ensuing Geopolymers Through Mechanical Activation’’, *Construction and Building Materials*, Vol. 57, pp. 151-162, 2014.

99. Kumar, S., R. Kumar, ‘‘Mechanical Activation of Fly Ash: Effect on Reaction, Structure and Properties of Resulting Geopolymer’’, *Ceramics International*, Vol. 37, No. 2, pp. 533-541, 2011.

100. Atalay, S., H. I. Adiguzel, F. Atalay, ‘‘Infrared Absorption Study of Fe_2O_3-CaO-SiO_2 Glass Ceramics’’, *Materials Science and Engineering A*, Vol. 304-306, No. 31, pp. 796-799, 2001.

101. Berzina-Cimdina, L. and N. Borodajenko, ‘‘Research of Calcium Phosphates Using Fourier Transform Infrared Spectroscopy’’, *Infrared Spectroscopy-Materials Science, Engineering and Technology*, ed. T. Theophanides, 2012.

102. Huang, C. K., P. F. Kerr, ‘‘Infrared Study of the Carbonate Minerals’’, *American Mineralogist*, Vol. 45, No. 2, pp. 311-324, 1960.

103. Yip, C. K., G. C. Lukey, J. L. Provis, J. S. J. Van Deventer, ‘‘Carbonate Mineral Addition to Metakaolin-Based Geopolymers’’, *Cement and Concrete Composites*, Vol. 30, No. 10, pp. 979-985, 2008.